POLITECNICO DI TORINO
Repository ISTITUZIONALE

Data scarcity in fatigue design of AM parts: A transfer learning framework to model the process structure property relationship

Original
Data scarcity in fatigue design of AM parts: A transfer learning framework to model the process structure property relationship / Centola, A., Ciampaglia, A., Paolino, D.S., Tridello, A.. - In: ENGINEERING FAILURE ANALYSIS. - ISSN 1350-6307. - ELETTRONICO. - 197:(2026). [10.1016/j.engfailanal.2026.111075]

Availability:
This version is available at: 11583/3013143 since: 2026-07-15T13:36:07Z

Publisher:
Elsevier

Published
DOI:10.1016/j.engfailanal.2026.111075

Terms of use:

This article is made available under terms and conditions as specified in the corresponding bibliographic description in the repository

Publisher copyright

(Article begins on next page)

06 November 2026

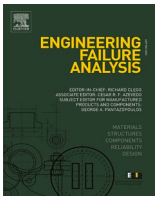
Engineering Failure Analysis 197 (2026) 111075



Contents lists available at ScienceDirect

Engineering Failure Analysis

journal homepage: www.elsevier.com/locate/engfailanal



Data scarcity in fatigue design of AM parts: A transfer learning framework to model the process – structure – property relationship☆

Alessio Centola *, Alberto Ciampaglia, Davide Salvatore Paolino, Andrea Tridello

Politecnico di Torino, Department of Mechanical and Aerospace Engineering, Torino 10129 Italy

ARTICLE INFO

Keywords:
Fatigue
Transfer Learning
Process Parameters
Additive manufacturing
Failure Prevention

ABSTRACT

The paper demonstrates the effectiveness of transfer learning (TL) in improving the fatigue failure prediction of additively manufactured (AMed) metallic alloys. The approach is applied to three commonly used AMed alloys – Ti6Al4V, AlSi10Mg and SS316L – to investigate the potential of multi-material knowledge transfer in improving the predictive accuracy under data-scarcity conditions, which are typical of fatigue testing. The TL framework employs a Bayesian neural network (BNN) pre-trained on data from two alloys and subsequently fine-tuned using data from the third, data-scarce alloy. Starting from the process parameters, risk volume, thermal and surface treatments, and the applied stress, the BNN predicts the fatigue life at a defined reliability (R) and confidence (C) levels. The TL effectiveness is assessed though a cross-material validation on the three alloys, by changing in turn the two alloys of the pre-training and the third as the target material with a truncated training dataset, mimicking realistic experimental scenarios with limited data availability. The model accuracy is evaluated using the R^2 score of the predictions on external validation datasets and is compared against the model trained without TL on the same reduced database. The results shows that TL improves both accuracy and generalization capability, benefiting from heterogenous multi-material knowledge, allowing to design against fatigue failures with greater confidence in this data scarce conditions. Moreover, TL enhances the ability to infer the influence of process parameters on fatigue behaviour, even when the available data are limited.

1. Introduction

Additive Manufacturing (AM) has rapidly advanced in recent years, enabling the production of lightweight and complex components [1–3] with previously unachievable geometries [4,5] such as lattice structures [6], with applications in the aerospace, biomedical, and automotive sectors [7–10]. Among metallic AM technologies, Laser Powder Bed Fusion (LPBF) is the most widely adopted for its precision and flexibility. Common alloys processed by LPBF include Ti6Al4V for its biocompatibility and strength, AlSi10Mg for its lightweight, and SS316L for its corrosion resistance. Despite these advantages, the fatigue performance of LPBF parts

☆ This article is part of a special issue entitled: 'ICAM 2025' published in Engineering Failure Analysis.

* Corresponding author.
E-mail address: alessio.centola@polito.it (A. Centola).

https://doi.org/10.1016/j.engfailanal.2026.111075
Received 12 March 2026; Received in revised form 25 May 2026; Accepted 3 June 2026
Available online 4 June 2026
1350-6307/© 2026 The Author(s). Published by Elsevier Ltd. This is an open access article under the CC BY-NC-ND license (http://creativecommons.org/licenses/by-nc-nd/4.0/).

is worse than that of conventionally manufactured counterparts [11–13]. The AM process originates several internal defects [14–16], such as lack of fusions and keyhole-induced porosities, and residual stresses induced by high thermal gradients, which further impair fatigue resistance. To mitigate these issues, several strategies can be adopted such as the optimization of process parameters [17], thermal and surface treatments [18,19], to reduce defectivity, improve surface quality, and relieve residual stresses. However, the combined influence of all these factors makes the characterization of the fatigue life of AMed parts highly complex. Traditional fatigue characterization relies on expensive and time-consuming experimental campaigns, thus designing experiments that include all the relevant factors is impractical [20]. To this end, Machine Learning (ML) can be employed as a powerful tool to tackle this complex multivariate problem [11,14,21–23]. In [24] a probabilistic guided learning approach has been used, with datasets with missing process parameters. In [25] 29 fatigue tests were carried out to link the influence of defects and stress amplitude on the life of AM Ti6Al4V using different ML algorithms. In [26] a physics informed ML approach was developed to associate the defect population to fatigue life, by assisting the training process with fracture mechanics theory. In [27] a finite element approach was embedded with ML algorithms, to better predict the fatigue performance of complex objects. In [28] a ML method driven by continuous damage mechanics was used to predict the fatigue life of AM AlSi10Mg parts. In [29] ML algorithms with SHapley Additive exPlanation values are used to predict the fatigue life of AMed SS316L specimens in as-built and post-treated manufacturing states. In [30] a non-destructive fatigue life prediction framework for AM alloys using a PINN and computed tomography techniques has been proposed. In [31] a PINN based on the Basquin equation is used to predict the high cycle fatigue life of AMed Ti6Al4V, while incorporating partial differential equations in the loss function. Moreover, the literature already contains large experimental datasets on fatigue of AM metals manufactured with different processing conditions. These datasets can be used to train ML models to reveal the intricate relationships between variables and fatigue life. Among ML methods, Neural Networks (NNs) are particularly suited to handle multivariate problems thanks to their flexibility and precision [32,33]. These can range from simple data-driven feed-forward neural networks (FFNNs) to physics-informed ones (PINNs) [25,33–37]. PINNs embed scientific laws in the loss function [38], providing superior capabilities in predicting the fatigue life [13,26,33,39–42]. NNs can also be declined into a probabilistic framework such as in [24,27] and [42], in which a Bayesian neural network (BNN) has been employed to separate the ML model uncertainty, tied to the BNN, from the epistemic and aleatoric uncertainty of fatigue, tied to the R90C90 life [43]. The use of BNN models, trained on R90C90 data, allows to estimate the uncertainty related to the training process [44] and provides more accurate and robust predictions. In fact, the BNN can output a distribution of R90C90 curves, from which the designer can choose a specific curve depending on the required confidence level of the industrial application. However, BNNs require large training datasets to achieve optimal performance, which poses a limitation due to the inherent challenges and cost of fatigue testing. On the other hand, the literature provides a wide range of fatigue test datasets for AMed alloys, which can be leveraged to overcome this issue. These datasets have been successfully used to train single material NNs [10,32,33,42]. However, for less commonly employed alloys, the available fatigue data in the literature remains limited, requiring dedicated experimental campaigns which are time-consuming and costly, and typically result in a reduced number of experiments.

This study investigates the use of transfer learning (TL) to overcome this limitation. TL allows to transfer knowledge from ML models pre-trained on one or more alloys to target alloys with limited data. Originally developed and widely adopted in image recognition, TL is now increasingly applied to materials science problems, where data scarcity is a pervasive challenge [10,45–47].

In the context of fatigue prediction for LPBF manufactured metals, TL can leverage similarities across different alloys and processing conditions to enhance predictive accuracy, even when the available training datasets are small, allowing to postpone fatigue failures even more. In [48], a TL model to predict the fatigue life of AMed SS316L with 109 training instances has been proposed. In [49] a TL-PINN framework has been developed to predict the fatigue life of mega-casting aluminum alloys by integrating the Paris' law and the M−integral method, with 21 data samples.

However, to the best of the authors' knowledge, no study employs a multi-alloy TL approach with approximately 2500 points spread across the most important AM alloys, such as Ti6Al4V, AlSi10Mg and SS316L, to improve the design trustworthiness against fatigue failures in data scarcity conditions.

The present paper introduces a probabilistic TL framework for fatigue life prediction of AM metallic alloys. BNNs pre-trained on two alloys are used to perform TL on a third alloy using a reduced database, simulating realistic scenarios where new materials are explored, but experimental failures are scarce. The study focuses on Ti6Al4V, AlSi10Mg, and SS316L, which are widely used in AM due to their favorable properties and abundant reference data. A wide multi-alloy training database has been created by aggregating data from over 70 papers, comprising approximately 2,500 datapoints organized into more than 220 datasets. To assess the effectiveness of TL, the predictive performance of the TL framework is compared against BNNs trained only on the reduced datasets of the target alloy, without TL. Model performance is evaluated using the R^2 accuracy score of fatigue life predictions, validated on external datasets excluded from the training phase.

The findings demonstrate that TL significantly improves both generalization and accuracy in fatigue failure prediction under conditions of data scarcity. Moreover, the developed TL framework allows a more reliable inference of the influences of the process parameters on fatigue behavior, when the training data are limited, allowing to improve the trustworthiness when designing against failures.

Section 2 describes the data source and modeling approach, including the composition of the training database and the fatigue models employed. Section 3 details the ML and TL methodology, outlining the structure of the BNN and the TL validation strategy. The results are presented and discussed in Section 4, where the advantages of employing TL across materials are analyzed as a function of the training data size, both with and without TL. Moreover, the ability of TL to infer the process parameters influence when the data are limited is also discussed in Section 5. Finally, Section 6 reports the conclusion of this study.

2. Data and models

This section outlines the database used to train the proposed BNN on Ti6Al4V, AlSi10Mg and SS316L (Section 2.1) and the fatigue models adopted to predict the fatigue life (Section 2.2).

2.1. Training database

In this section, the training database used in the study is discussed. Since the cyclic performance of these AM alloys is dependent on the inherited manufacturing defects and these ones depend in turn on the manufacturing process, the process parameters, the risk volume (V_{risk}), and the thermal and surface treatments must be considered in the database. As the LPBF process undergoes, a laser beam, with a given power P [W] and scanning speed v [mm/s], gradually melts the alloyed powder on a pre-heated platform, with equally spaced passes, as dictated by the hatch distance h [μm]. This process is repeated for each layer, as the building platform lowers by a quantity named layer thickness t [μm]. The mechanical properties of the specimen are also influenced by its orientation ϑ [°] on the building chamber (horizontal 0°, inclined 45° and vertical 90°). The database includes a heterogeneous distribution of process parameters for the three alloys and their ranges are reported in Table 1. To have a coherent and continuous training database, while ensuring also a sufficiently high number of training instances, only the input features consistently reported across all datasets were retained.

To model the influence of the size effect [19], the risk volume V_{risk} has been calculated as described in [41]. This also allows the different specimens' geometries and fatigue test types to be taken into account as a single training feature. Thermal treatments, as annealing and hot isostatic pressing (HIP), are often applied to reduce the high thermal stresses and the defect population of as-built parts. The combination the chosen process parameters with the thermal treatments determines the final microstructure of the AMed part. The application of these two treatments is denoted with Boolean values (TT_Ann and TT_HIP) along with their temperature (T_Ann and T_HIP [°C]), duration (dt_Ann and dt_HIP [hours]) and pressure (P_HIP [bar]). Given the improvement on the fatigue performance induced by the surface treatments on the rough surface finish of as-built parts, they have also been considered to improve the accuracy of the BNN, again as Boolean features. The considered surface treatments are 13 in total and they are related to the three investigated materials: namely, machining (ST_Mac), polishing (ST_Pol), grinding (ST_Grind), sand blasting (ST_SB), shock peening (ST_SP), laser shock peening (ST_LSP), friction stir processing (ST_FSP), vibratory finishing (ST_VF), surface mechanical attrition (ST_SMAT), nitriding (ST_Nitr), deep nitriding (ST_DN), electric discharge machining (ST_EDM) and electro polishing (ST_EP). Variables such as the static properties, microstructure characteristics or thermal coefficients of the alloys have not been used as input features because they are an output of the process. Moreover, given that standard alloys have been considered, their chemical composition variability is quite small and its influence on the fatigue life, can be assumed to be already included in the experimental scatter captured by the R90C90 formulation. For each dataset the process parameters, V_{risk} and the post treatments have been reported in Table A of Appendix A, with the number of specimens. N_f ranges from 10^2 to 10^9, with most of the data in the high cycles fatigue region, whereas S_a from 50 MPa to 850 MPa. With this, the proposed TL framework can model the fatigue behavior below 10^7 cycles. The very high cycle fatigue regime could have also been modeled provided that enough data is available. The Smith-Watson-Topper correction is applied to account for the stress ratio R influence and the different loading conditions. The database (Table A) is made of a total of 2498 points: 1106 for Ti6Al4V, 874 for AlSi10Mg and 518 for SS316L. The total number of datasets is 222 coming from 71 literature papers: 88 datasets from 32 articles for Ti6Al4V, 83 datasets from 22 papers for AlSi10Mg and 51 datasets from 17 articles for SS316L, with all literature sources providing data for a single alloy only. Fig. 1 shows all the data points in the database on the SN plane, clustered by alloy composition, including both failures and runouts.

2.2. Fatigue model

The BNN used for the TL application is trained to predict a statistical estimation of the fatigue life at a defined reliability and confidence level. The statistical methods used to derive the reliability and confidence intervals from the experimental data are outlined in the following. The adopted fatigue model is the Basquin's law with a Normal distribution [50] in the bi-logarithmic stress life plane, with N_f being the random variable, mean $\mu = a + b \cdot log_{10} S_a$ and standard deviation σ, with a and b being the intercept and slope coefficients. The cumulative distribution function, F_{N_f} (Eq. (1)), reads:

$$F_{N_f} = \Phi\left[\frac{\log_{10} N_f - (a + b \bullet \log_{10} S_a)}{\sigma}\right], \tag{1}$$

Table 1
Process parameters ranges for Ti6Al4V, AlSi10Mg and SS316L alone and together.

Process parameter	Ti6Al4V	AlSi10Mg	SS316L	All
Power P [W]	95 – 450	175 – 490	90 – 350	90 – 490
Scan speed v [mm/s]	150 – 1900	500 – 2667	425 – 2400	150 – 2667
Hatch distance h [μm]	50 – 180	61 – 200	60 – 150	50 – 200
Layer thickness t [μm]	20 – 60	25 – 60	20 – 50	20 – 60

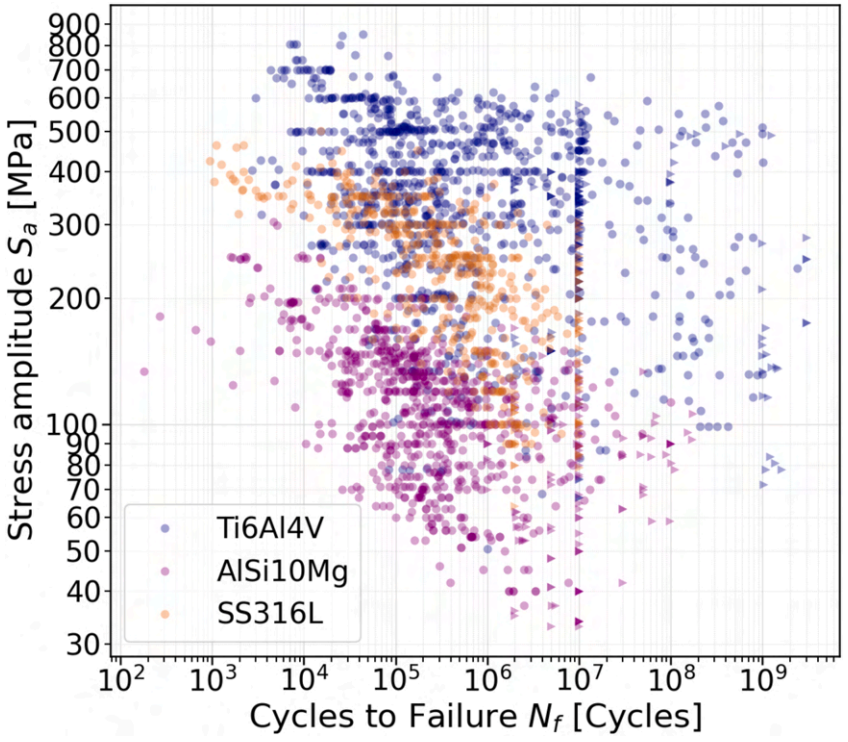


Fig. 1. All the points belonging to the training database shown in the SN plane for Ti6Al4V, AlSi10Mg and SS316L. Circular markers refer to failures, whereas triangular ones to runouts.

The R50 expression is determined by minimizing the negative log-likelihood (NLL) as in Eq. (2), where both N_f and S_a are referred to as their base-10 logarithmic versions:

$$NLL = -\sum_{i=0}^{M}(1-R_{f,i}) \bullet \ln\left(f_{N_f}\left[\log_{10}N_f;\, a+b\bullet\log_{10}S_a,\, \sigma\right]\right) + R_{f,i} \bullet \ln\left(1-F_{N_f}\left[\log_{10}N_f;\, a+b\bullet\log_{10}S_a,\, \sigma\right]\right), \tag{2}$$

with M being the number of specimens, $R_{f,i}$ the runout flag for *i-th* specimen [43], F_{N_f} the cumulative distribution function and f_{N_f} the probability density function. Once a, b and σ have been estimated, the Probabilistic S-N (PSN) curves of the dataset can be determined for the selected reliability level.

To model the confidence intervals, the BNN predicts both the R50 curve as well as the R90C90 curve, usually adopted in industrial practice. This allows to separate the experimental uncertainty of the training data from the ML model uncertainty, as discussed in [42]. To estimate the R90C90 curve, the Owen's procedure [43], which provides the k_{Owen} coefficient, is used to shift downward the R50 curve by a quantity equal to $k_{Owen} \bullet \sigma$, providing a modified value of the intercept, a_{R90C90}. Since fatigue failures in AMed parts are mainly caused by defects, their presence is implicitly taken into account by the BNN trained on experimental fatigue failures, as shown in [10]. The microstructure also plays a role in affecting the fatigue performance, but less critically compared to AMed defects. Accordingly, these latter ones introduce scatter in the experimental results and this variability is accounted using a probabilistic fatigue model. To counteract fatigue failures caused by defects, design fatigue curves that account for different failure mechanisms and sources must be considered. Therefore, it is necessary to employ R90C90 design fatigue curves, which are modelled probabilistically and include the influences of both defects and microstructure on the cyclic response and the presence of different failure causes. Moreover, the R90C90 formulation already accounts for physics-informed constraints, that not only allows to account for the experimental variability presents in fatigue failure causes, such as defects and microstructure, but also constraints the BNN predictions to be strictly linear and monotonically decreasing at the same time. On the other hand, raw neural network predictions would lead to unphysical behaviours such as the fatigue life increasing as the stress amplitude increases, as discussed in [33].

3. Transfer learning algorithms

This section outlines the TL framework employed in this study. Section 3.1 details the BNN. Section 3.2 describes the TL training techniques, and Section 3.3 introduces the validation strategy.

3.1. Bayesian neural network model architecture

The BNN is composed of one input layer, 3 hidden deterministic layers and 1 output mixed layer. The input layer has 27 input nodes grouped under 5 categories, reflecting the training database of Table A, as shown in Section 2.1: process parameters (5 inputs), V_{risk} [mm^3], thermal treatments (7 inputs), surface treatments (13 inputs), and S_a [MPa]. The process parameters are ϑ [°], P [W], v [mm/s], h [μm] and t [μm]. The surface treatments are encoded as Boolean features using the one-hot strategy. For the thermal treatments, TT_Ann and TT_HIP are Boolean features, while T_Ann [°C], T_HIP [°C], dt_HIP [hours], dt_Ann [hours] and P_HIP [bar] are numeric. The microstructure is also implicitly modeled as it is influenced by the combination of process parameters and thermal treatments. All the inputs are represented in the 5 categories of Fig. 2 and are fed into a pyramidal structure of three hidden deterministic layers (Fig. 2 in green) of respectively 100, 75 and 50 nodes, all activated with a ReLU function. This pyramidal structure has proven to be effective in predicting the fatigue life of LPBF components [32–34,42]. Moreover, the input node of S_a is concatenated to the third layer to give it a higher importance, given that S_a influences the life much more with respect to the other inputs, and to establish the correct linear relation between S_a and N_f. The 3rd layer is connected to the linearly activated output variational layer, which provides the prediction of both the R50 and R90C90 life (N_f and $N_{f,R90C90}$), while ensuring an improved model generalization [44]. The BNN allows also to separate the ML model uncertainty linked to the heterogeneity of literature data, from the epistemic and aleatoric uncertainty of fatigue, captured by the R90C90 life. In fact, a BNN can capture the ML model uncertainty by considering Bayesian statistics as part of the model architecture, with at least one variational layer. This latter one is defined by the activation function, number of neurons, prior and posterior distributions type, as well as the Kullback-Leibler (KL) weights [51]. Unlike a FFNN or a PINN, the parameters of a variational layer are treated as random variables as opposed to single deterministic values. The connections between a variational layer and its previous one are, in this study, modelled by a multivariate Normal distribution, whose prior is initialized to a standardized multivariate distribution (null mean vector $\underline{\mu} = \underline{0}$ and identity covariance matrix $\underline{\Sigma} = \underline{I}$) and updated to a fully populated posterior, as training progresses. This is done by maximizing the log-likelihood of the posterior distribution on the available training data while decreasing the KL divergence, as shown in [44]. The BNN is first pre-trained for 1500 epochs with a learning rate of 0.001 and 15 steps per epoch, with a training and testing split of 90%-10%, whose testing split is used to evaluate the generalization capabilities of the model. This split has been chosen, as opposed to an 80%-20% one, due to the relatively limited database size, which becomes particularly relevant for the reduced databases of 50, 100, 150 and 200 training points, as discussed in Section 3.3. Nevertheless, the adopted split becomes of secondary importance given that the assessment of the effectiveness of TL has been performed on datasets that are always external to the partitioned databases of reduced size, which constitutes a severe validation procedure as explained in Section 3.3. Additional studies regarding the chosen train-test split have been reported as supplementary materials, in which analyses comparing the adopted 90%-10% split with the 80%-20% split have been performed.

3.2. Transfer learning techniques

The TL procedure (Fig. 3) starts with the pre-training of the BNN on a fully-populated database of two different alloys.

Then, the pre-trained BNN is loaded (Fig. 3, step 1), with the weights w_{ij} and biases b_i saved from the last training epoch. This BNN has been pre-trained on a relatively large amount of training data. As an example, if TL is applied on the data-scarce alloy A, firstly a BNN is trained with the available data of other alloys (alloy B and C) and then loaded. In step 2, the three intermediate layers of the BNN are frozen and the output one is left trainable (Fig. 3, step 2). In this way, the latent relationship learned from the previous alloys is preserved, while the last unfrozen layer can adapt to the new training data of the data-scarce alloy. Then, the partially-frozen BNN is trained for a reduced number of epochs, (e.g., 200 epochs for training against 1500 epochs for pre-training), with the same learning rate and number of steps per epoch (Fig. 3, step 3) of respectively 0.001 and 15. Finally, the three hidden layers are unfrozen (Fig. 3, step 4), and a fine-tuning training is performed for five epochs on the same training data of step 3, using a much smaller learning rate

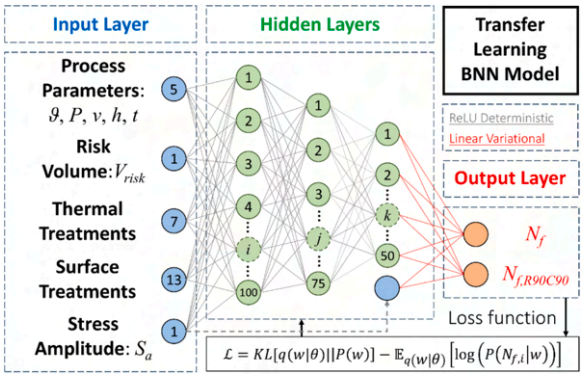


Fig. 2. Adopted BNN architecture for the TL application. The blue circles are the input nodes, the green the hidden ones and the orange the output ones. In grey, the hidden layer deterministic ReLU connections. In red, the output layer variational connections for both the R50 and the R90C90 life.

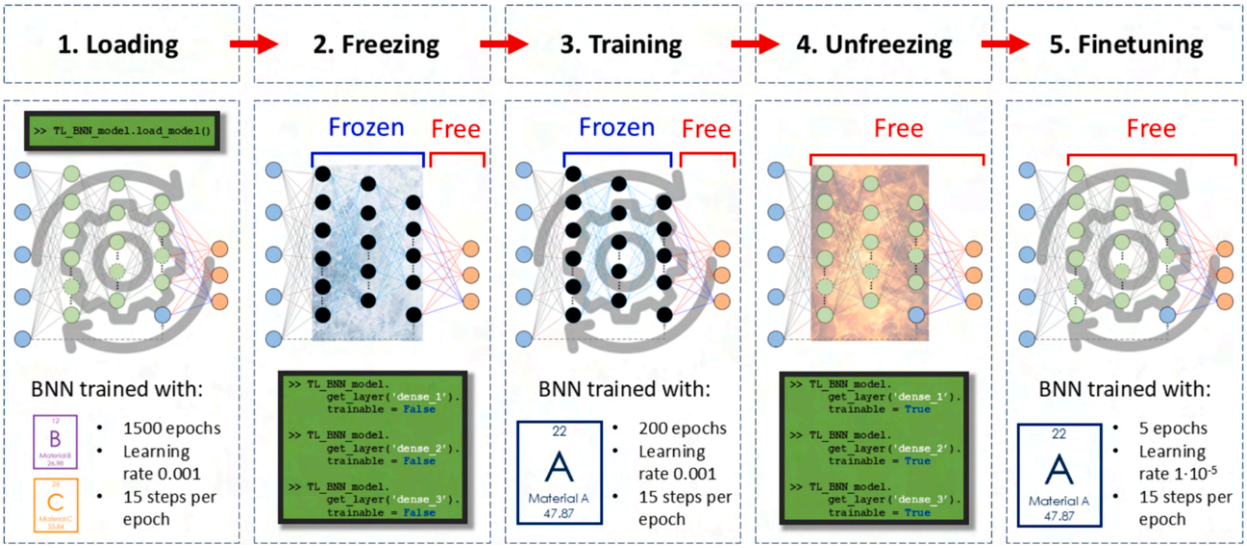


Fig. 3. Transfer Learning training workflow from material B and C to material A with the employed BNN model.

40 trainings without TL

40 trainings with TL

Training sessions per TL case	1	2	3	4	...	4*i*+1	4*i*+2	4*i*+3	4*i*+4	...	37	38	39	40
Material A Dataset X	Combination 1				...	Combination *i*				...	Combination 10			
Datasets code The analyzed dataset X (e.g. dataset 2) for material A, is never inside the training data	4	4	4	4	...	28	28	28	28	...	13	13	13	13
	60	60	60	60		5	5	5	5		7	7	7	7
	23	23	23	23		33	33	33	33		62	62	62	62
	45	45	45	45		19	19	19	19		48	48	48	48
		38	38	38		41	41	41	41		59	59	59	59
		11	11	11			1	1	1		25	25	25	25
		27	27	27			63	63	63			3	3	3
			31	31			38	38	38			9	9	9
			28	28				70	70			35	35	35
			8	8				3	3			26	26	26
			56	56				15	15				53	53
			0	0					65				45	45
				35					23				32	32
				42					37				21	21
				67					55					4
				22					26					36
														18
N° rounded	50	100	150	200	...	50	100	150	200	...	50	100	150	200
N° actual	52	107	155	203		54	101	150	202		50	103	156	204
R50 and R90C90 Without TL & With TL	R^2 evaluated on External Validation Dataset 2				...	R^2 evaluated on External Validation Dataset 2				...	R^2 evaluated on External Validation Dataset 2			

Fig. 4. Strategy adopted to create the databases of reduced size to assess the effectiveness of TL on the studied alloy A. These databases of progressively increasing numerosity are built on entire datasets and amount to respectively 50, 100, 150 and 200 points approximately, with each of them having 10 combinations of training datasets.

(Fig. 3, step 5). Although optional, this fine-tuning procedure smoothens the variations between the training sessions while further improving the generalization capability.

3.3. Validation of the effectiveness of transfer learning

To simulate the data-scarcity of experimental failures and cross-validate the effectiveness of TL, several training databases are built by sub-sampling the full database. Precisely, four training databases with progressively increasing numerosity are obtained for the target material, with 50, 100, 150 and 200 points approximately. Data are sampled by randomly selecting experimental datasets, rather than being randomly drawn point by point, to simulate the actual production of specimens that are batch-produced with the same set of process parameters. To preserve continuity while creating the next database, 50 more points are added while the previous ones are preserved, up to 200 points are reached, always by adding full datasets. This has been done to understand if there is an appreciable increase of accuracy thanks to TL, as the number of training points increases. To mitigate the effects of randomness, a cross-validation with 10 combinations of these 4 databases of progressively increasing numerosity has been performed, resulting in a total of 40 combinations (Fig. 4). To corroborate the effectiveness of TL, an ablation study has been performed with the same training conditions previously explained, but without the application of TL. In this context the ablation consists in the omission of the initialization given by the pretrained BNN and of the finetuning and not in the removal of parts of the BNN model, when TL is not applied. This allows to isolate the contribution of TL to assess the predictive performance differences when TL is omitted. The creation of the reduced size databases is not part of ablation itself, rather it has been introduced to simulate data scarcity in realistic fatigue testing conditions. Therefore, to assess the effectiveness of TL, for each of the ten combinations of a given numerosity, a training session is performed with TL (as in Fig. 3), and without TL. This results in a grand total of 80 training sessions and 80 BNNs, 40 with TL and 40 without TL. After each training session, a dataset external to the training database is evaluated by the 80 BNNs. Accordingly, this type of evaluation is severe, as the external dataset is never seen during training, therefore the TL algorithm is blindly evaluated. Each BNN predicts both the R50 and R90C90 curves of the external dataset, which are then averaged over the 10 training combinations. As a result, for each validation dataset, and for each numerosity, there are 4 representative PSN curves (averaged over the 10 combinations): 4 R50 curves with TL, 4 R50 curves without TL, as well as 4 R90C90 curves with TL and 4 R90C90 curves without TL; 16 in total. This study on this progressively increasing number of data has been done to assess an ideal number of training data from which TL starts being effective, as it will be discussed in Section 4.1.

To assess the accuracy of the predictions, the R^2 score is calculated for each curve with respect to the experimental points of the external validation dataset. These R^2 are then normalized with the experimental R^2 of the R50 line as in Eq. (3), whose value is the highest possible one.

$$R^2_{BNN,norm,R50} = \frac{R^2_{BNN,R50}}{R^2_{exp,R50}}; \tag{3}$$

These normalized $R^2_{BNN,norm}$ values of the procedure, with and without TL, for the four dataset sizes, are compared to assess the convenience of TL, as shown in Fig. 5. According to this severe validation procedure, where the evaluated dataset is always outside the training and testing dataset fed to the BNN while training, the results are highly unbiased. The R^2 score has been chosen as a validation metric as it is more suitable to evaluate the fitting accuracy of linear fatigue models on experimental datasets, given that the effectiveness of TL is assessed by datasets, to mimic actual fatigue testing campaigns.

A very important note concerns feature normalization. In the following research, all the numeric features and labels are normalized according to the Z-score formula ($x_{i,norm} = (x_i - \mu_x)/\sigma_x$). However, it is important to correctly represent feature scaling with respect to the past training history of the BNN. If TL is not applied, this is not a critical issue as the features are normalized with respect to μ and σ of the few training datasets of alloy A. However, if TL is applied, all the new features of the new alloy A, must be scaled with respect to the μ and σ of the new and the past data, hence they are calculated on the entire data of alloy B and C related to the pre-trained BNN, as

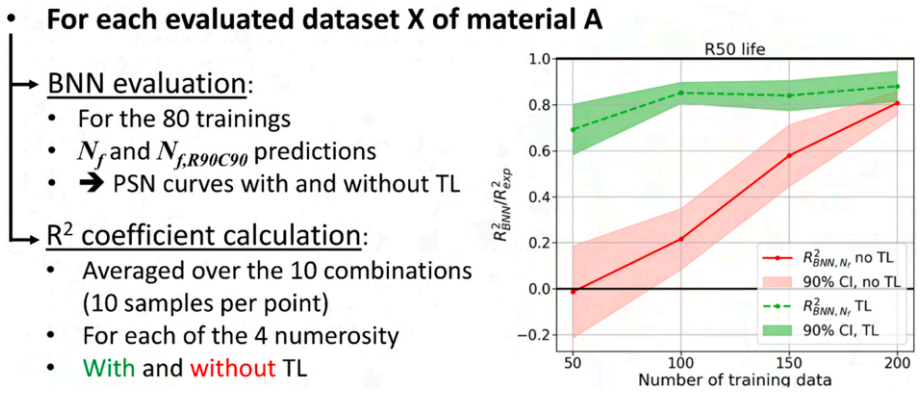


Fig. 5. TL effectiveness evaluation strategy via $R^2_{BNN,norm}$ coefficients for an external dataset X of material A.

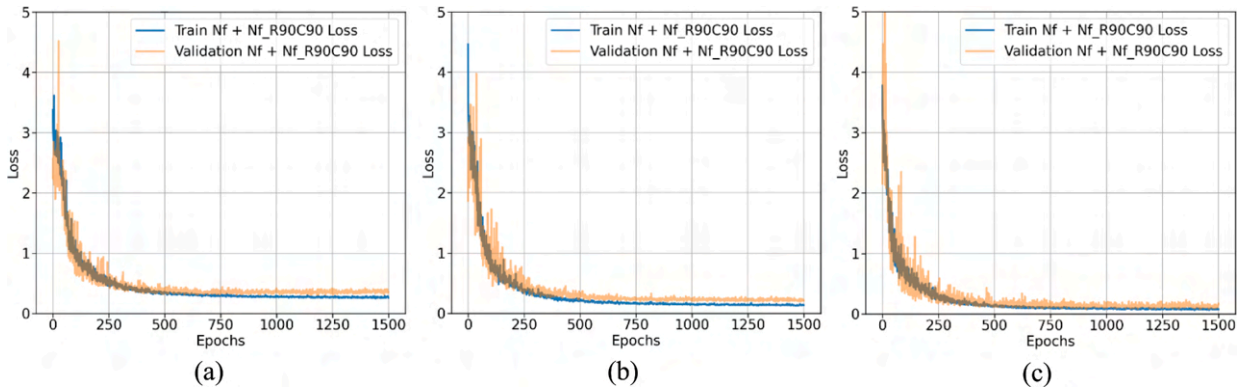


Fig. 6. Training and validation losses of the R50 and R90C90 life BNNs trained on AlSi10Mg and SS316L (a), Ti6Al4V and SS316L (b), and Ti6Al4V and AlSi10Mg (c).

well as on the considered reduced training database of alloy A. If this is not done, the results are incorrectly represented. The so-called "alloy A" is studied as to be all three alloys on rotation, namely Ti6Al4V, AlSi10Mg and SS316L. It follows that the BNN from which TL is performed as a starting point is trained on the other two remaining materials. As an example, if the effectiveness of TL is tested on Ti6Al4V, the loaded BNN is trained on AlSi10Mg and SS316L, and so on for the other two alloys on rotation.

4. Results

In this Section, the BNNs with and without TL are compared, to show the enhancement of the predictive capabilities to design against failures. To study the ablation of TL, the performance of each BNN is analyzed by considering each PSN curves and the corresponding $R^2_{BNN,norm}$ score, when TL is applied to Ti6Al4V (Section 4.1), AlSi10Mg (Section 4.2), and SS316L (Section 4.3). Fig. 6 reports the training metrics of the three pre-trained BNNs, combining both the R50 and R90C90 losses. A cross-validation study with 100 training sessions has been performed for each of the three cases, and among those, the ones with the lowest training and generalization errors have been selected. Fig. 6a reports the metrics of the BNN trained on AlSi10Mg and SS316L to perform TL on Ti6Al4V. Fig. 6b refers to the BNN trained on Ti6Al4V and SS316L for the TL of AlSi10Mg, whereas Fig. 6c shows the metrics of the BNN trained on Ti6Al4V and AlSi10Mg for the TL of SS316L. It can be observed that for all three BNNs, both the training and validation losses have a steep descent, with the latter being slightly above the former. This is a sign that the BNNs are well generalized and do not risk overfitting [52].

The following Sections report, for each material, the PSN curves and the R^2_{norm} scores obtained with increasing number of training data. Additional error metrics along with parity plots, were reported as supplementary materials to further quantify the prediction accuracy of the model. Mean absolute error (MAE) and mean squared error (MSE) were calculated on the predicted N_f values for the selected external validation datasets, with and without TL, and for all investigated training sizes.

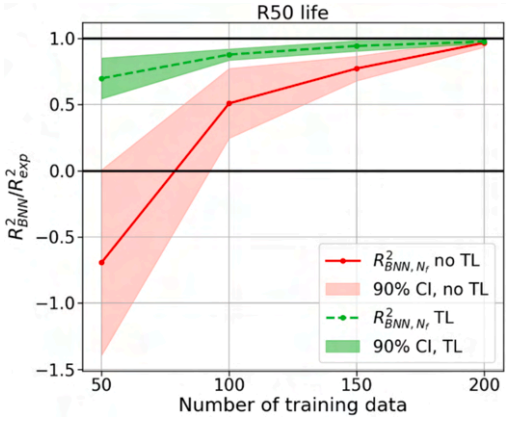


Fig. 7. $R^2_{BNN,norm}$ vs. number of training datapoints with the 90% confidence interval of the mean for the Ti6Al4V validation dataset 38, for the R50 life. In red the case without TL, while in green the case with TL applied.

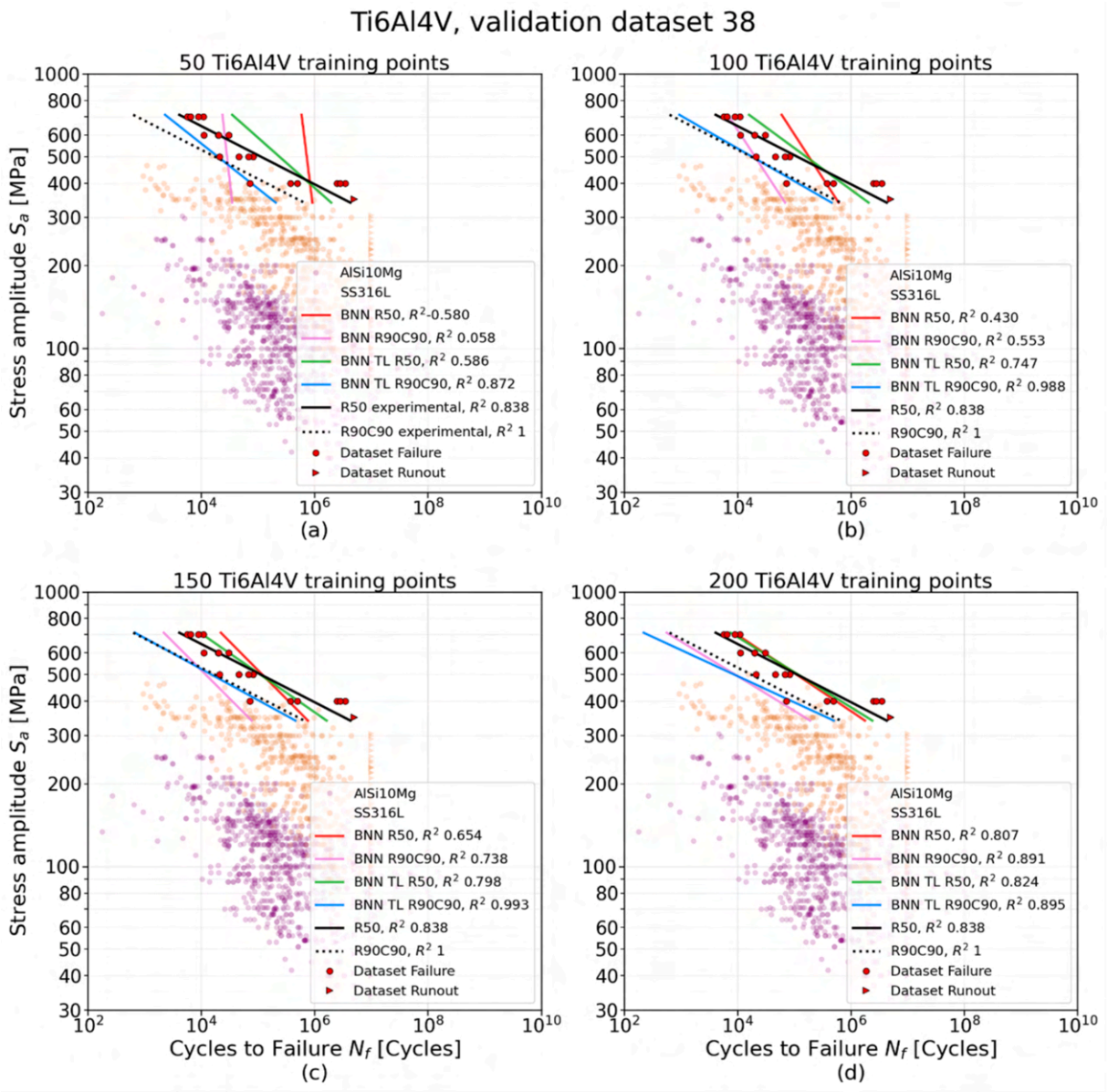


Fig. 8. PSN curves to assess the effectiveness of TL on Ti6Al4V from a BNN pretrained on AlSi10Mg (purple points) and SS316L (orange points). The external dataset 38 (red points and triangles) has been validated with combinations of 50 (a), 100 (b), 150 (c) and 200 (d) training points to output the R50 (red without TL and green with TL) and R90C90 life (magenta without TL and blue with TL) with and without TL. In solid black the experimental R50 line, while in dashed black the experimental R90C90 line.

4.1. Ti6Al4V

To assess the effectiveness of TL on Ti6Al4V, 14 external validation datasets have been blindly evaluated. However, since 4 SN diagrams (one for each numerosity) must be shown to assess the effectiveness of TL, only one validation dataset is shown for the sake of conciseness. For Ti6Al4V, the external dataset 38 is shown as an example [53] (Table A). Considering a dataset, for each numerosity (50, 100, 150 and 200), 10 training sessions have been performed, each with a random combination of training datasets, with and without TL (Fig. 4). For each training case, the $R^2_{BNN,norm}$ of N_f is evaluated starting from the PSN curves predicted by the BNN, which are averaged over the 10 training data combinations. Fig. 7 shows the results of the mean of the R^2_{norm} with its 90% confidence interval, while increasing training datapoints for N_f.

For each database size (50, 100, 150, and 200), the 90% confidence interval of the mean can be plotted with its average $R^2_{BNN,norm}$ value computed over 10 randomly initialized training, both with and without TL. Being this a normalized version of the R^2 coefficient, values equal to one mean that the curve predicted by the BNN has the same fitting accuracy of the experimental one, which is the best

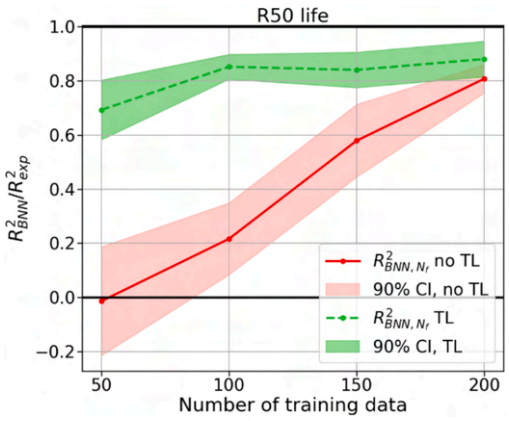


Fig. 9. $R^2_{BNN,norm}$ vs. number of training datapoints with the 90% confidence interval of the mean for the AlSi10Mg validation dataset 55, for the R50 life. In red the case without TL, while in green the case with TL applied.

possible prediction on the evaluated experimental validation dataset. It can be clearly observed that the case with TL always provides more accurate predictions for each numerosity, as its curve is always above its traditionally trained counterpart without TL. It is also evident how increasing the number of training points leads to an increase in precision and, more generally, to a reduction in scatter, both with and without TL. Fig. 7 shows that TL yields a normalized accuracy $R^2_{BNN,norm}$ close to 0.7 of the R50 estimates with only 50 training points, while standard training fails, as indicated by the $R^2_{BNN,norm}$ without TL. The TL prediction with 100 datapoints shows an improvement, with respect to the prediction without TL. The benefit of TL is less prominent as the number of data increases up to 200, where the $R^2_{BNN,norm}$ without TL approaches the one obtained with TL. The consistent increase of the R^2 scores obtained with TL with small training datasets proves its effectiveness in improving the accuracy of the predictions when the data is scarce. Furthermore, when using TL, the R^2 score quickly saturates as the number of training points increases, allowing to reduce the size of the experimental dataset. Moreover, TL positive effect is confirmed by the fact that the confidence intervals of the mean values do not overlap. Accordingly, this difference is statistically significant.

Fig. 8 shows the prediction of the fine-tuned BNN for the validation dataset, averaged over the 10 training combinations. The prediction for the R50 and R90C90 curves are compared with the experimental data, the fitted fatigue model, and the BNNs trained only on the reduced database (without TL). The predictions are shown for 50 (Fig. 8a), 100 (Fig. 8b), 150 (Fig. 8c) and 200 (Fig. 8d) training points. In purple and orange are shown the experimental failures and runouts points used for the pre-trained BNN, belonging respectively to AlSi10Mg and SS316L. Indeed, it can be observed how the case with TL provides S-N curves that are closer to their experimental counterparts as opposed to the case without TL, for all cases, with a precision that is increasing as the number of training points increases. Moreover, for the case with 50 training points, the R90C90 line with TL (Fig. 8a, blue line) can already be used to safely design components against fatigue failure, as each experimental point of the external validation dataset falls above it. For Ti6Al4V, it can be concluded that this method is robust and trustworthy, especially with such severe validation conditions, where the pre-trained BNN never sees the evaluated material and the TL BNNs never consider the external validation dataset. Other PSN curves of additional Ti6Al4V external datasets evaluated at 50 training points are reported in Fig. B1 of Appendix B.

4.2. AlSi10Mg

For the validation on AlSi10Mg, 16 external datasets have been validated. Here, as an example, the results on the external dataset 55 are shown in Fig. 9 with the $R^2_{BNN,norm}$ mean and its 90% confidence interval. The $R^2_{BNN,norm}$ mean score of the R50 life with TL is around 70% with only 50 datapoints, while the predictions without TL are significantly inferior, with a mean score close to zero. As the number of training points increases, the $R^2_{BNN,norm}$ score achieves a stable behavior around 90% for the case with TL, outperforming the case without TL, which shows worse predictive capabilities. Once again, the fact that the confidence intervals of the mean do not overlap, especially at a low number of training points, proves that the positive effect of TL is also statistically significant.

By inspecting the PSN curves (Fig. 10), the TL positive effect is also observable, as at a low number of training points, such as 50 (Fig. 10a) and 100 (Fig. 10b), the R90C90 curve with TL can provide accurate predictions for fatigue design. On the other hand, the case without TL needs 200 data points to provide a sufficient accuracy of the R90C90 curve (Fig. 10d). Additional results predicted by TL at 50 training points on four more AlSi10Mg external datasets are reported in Fig. B2 of Appendix B.

4.3. SS316L

For SS316L 11 external datasets have been blindly validated. SS316L is the alloy to benefit the most out of TL, since its TL is performed from a BNN trained with the highest number of data (1106 for Ti6Al4V plus 874 for AlSi10Mg). Moreover, its dataset points are located between well-populated regions of the SN diagram (Fig. 1), given that SS316L has intermediate performances compared to Ti6Al4V and AlSi10Mg. Indeed, this can be confirmed by Fig. 11, by studying the SS316L external validation dataset 41, in which it can

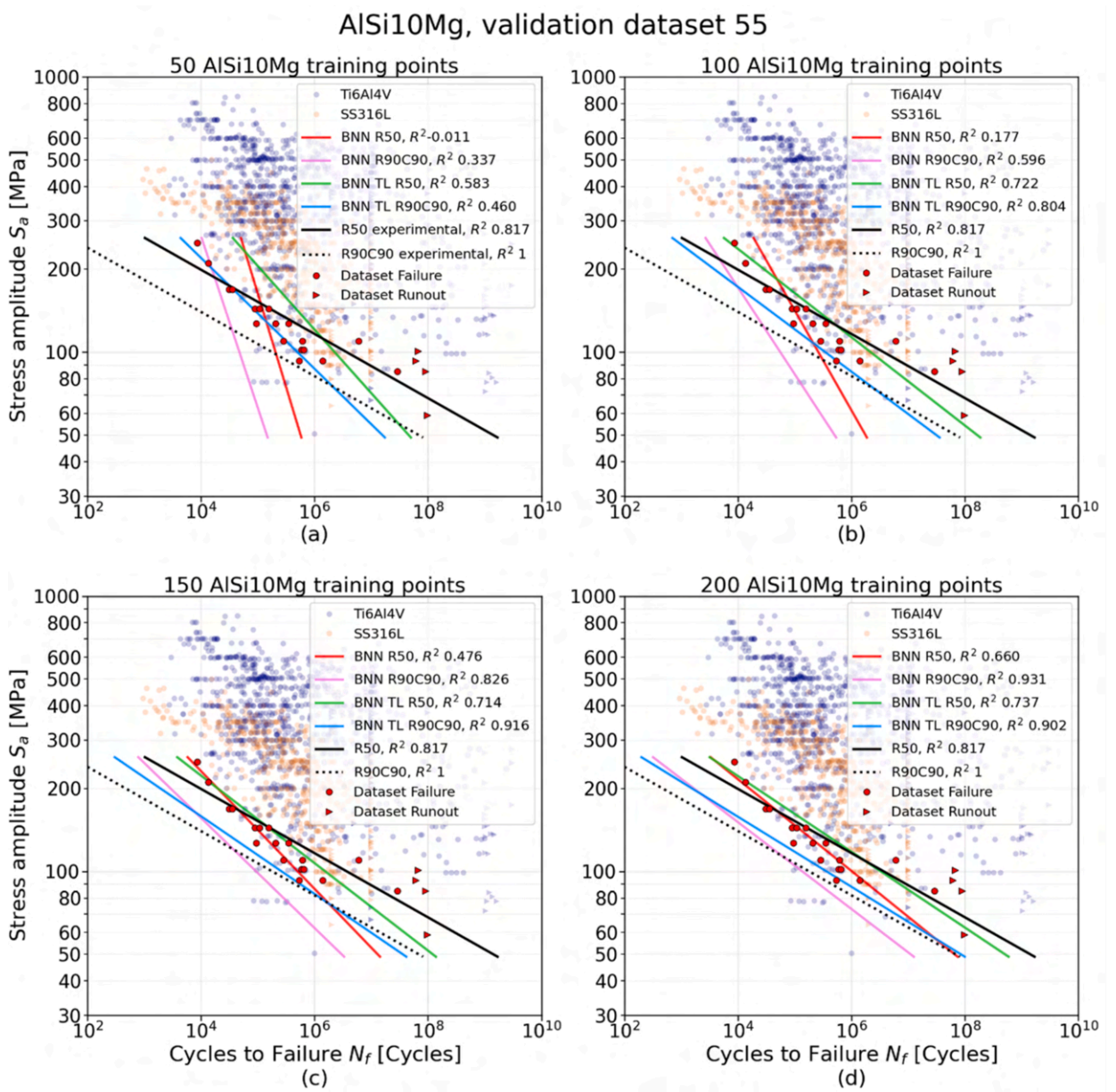


Fig. 10. PSN curves to assess the effectiveness of TL on AlSi10Mg from a BNN pretrained on Ti6Al4V (blue points) and SS316L (orange points). The external dataset 55 (red points and triangles) has been validated with combinations of 50 (a), 100 (b), 150 (c) and 200 (d) training points to output the R50 (red without TL and green with TL) and R90C90 life (magenta without TL and blue with TL) with and without TL. In solid black the experimental R50 line, while in dashed black the experimental R90C90 line.

be seen that TL gives a significant head-start when the number of data is as low as 50 for the R50 life $R^2_{BNN,norm}$ scores, with mean values above 80%. The behavior saturates to a very accurate prediction for the remaining cases with 100, 150 and 200 datapoints. The case without TL struggles to provide reliable predictions for all the database sizes, as its mean value saturates close to 60%. Also for SS316L, the TL positive effect is particularly evident and it is confirmed by the fact that the confidence interval of the mean for the case with TL is very far from the one of the case without TL. Accordingly, this difference is particularly significant statistically speaking even for SS316L.

This can indeed be confirmed from the PSN curves of Fig. 12. No particular difference is observed between the R50 and R90C90 lines with TL (green and blue lines) at different number of training points. Therefore, 50 training points can be used with confidence to reliably design against fatigue failures, as the R90C90 line (Fig. 12a, blue line) is very close to its experimental counterpart. The same holds for the higher number of training points, even though it is obviously more convenient to employ fewer training points, as in Fig. 12a. The case without TL struggles significantly in providing trustworthy predictions, with a barely usable R90C90 line only in the

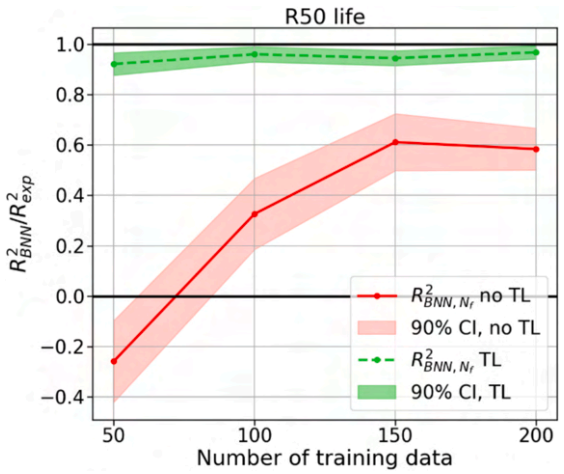


Fig. 11. $R^2_{BNN,norm}$ vs. number of training datapoints with the 90% confidence interval of the mean for the SS316L validation dataset 41, for the R50 life. In red the case without TL, while in green the case with TL applied.

200 training points case (Fig. 12d purple line). Moreover, Fig. B3 of Appendix B shows four more PSN curves of SS316L external datasets evaluated at 50 training datapoints.

5. Discussion

From the results reported in Section 4, the TL effect is particularly evident and beneficial already at a low number of training points such as 50, which are more conveniently obtained with respect to a higher number of points. Therefore, designers can greatly benefit from the application of TL already at a low number of fatigue specimens. To corroborate this statement, additional PSN curves evaluated at 50 training points on other external datasets are reported in Appendix B for all alloys. Nevertheless, to have a complete perspective on the assessment of the effectiveness of TL at 50 training points, Fig. 13 reports the normalized R^2 score averaged over all the external validation datasets (14 for Ti6Al4V, 16 for AlSi10Mg and 11 for SS316L), along with its 90% confidence interval, for all alloys, both for the R50 and R90C90 life. It can be clearly seen that TL allows to deliver a significant improvement in precision with respect to its traditionally trained counterparts for all alloys, given its lower prediction error. As stated in Section 4.3 this effect is particularly beneficial for SS316L, followed immediately after by Ti6Al4V and then AlSi10Mg. The TL from Ti6Al4V and SS316L to AlSi10Mg is still effective but not as much as for the other two alloys. This is because AlSi10Mg is positioned below the other two alloys in the SN diagram (Fig. 1), since, for the same N_f, AlSi10Mg exhibits a lower S_a with respect to the other two alloys, which can limit the effectiveness of knowledge transfer. Nevertheless, the employment of TL is beneficial even to counteract fatigue failures for AlSi10Mg. Moreover, the positive effect of TL is supported by the absence of overlap between the confidence intervals of the means for all alloys at 50 training points, suggesting that the observed difference is statistically significant.

The following approach, based off the gathered and available literature data, is only applicable to bulk AM parts, not to lattice structures. However, it can be extended to the latter, provided that sufficient training data on lattice structures are available or that TL is applied to them. Once TL has been assessed to be effective, the process parameter influence on the fatigue life can be discussed along with the capabilities of TL to infer such influences from other alloys when the training data is limited. Section 5.1 presents a complete layout of the influence of the process parameters (namely ϑ, P, v, h and t) on the fatigue life for the three alloys, whereas Section 5.2 investigates the effectiveness of TL in inferring the process parameter influence on the life from other alloys.

5.1. Process parameters influence on fatigue life

For each alloy, and for every set of process parameters, the evaluation was carried out using a constant set of input features, with the exception of the process parameter under study, which was varied across its range of interest, as illustrated in Table 1. The constant features are set to the most recurrent values, as reported in Table 2. All thermal and surface treatment variables were set to zero, ensuring that the analysis referred exclusively to the as-built condition. These choices were made to minimize the influence of data availability and to isolate the specific effect of the process parameters on the fatigue behavior.

Given that each of the three alloys has different ranges of S_a, two representative S_a levels were selected for each alloy, chosen where a larger amount of data was available (Fig. 1). Specifically, Ti6Al4V was analyzed at 300 and 500 MPa, AlSi10Mg at 100 and 200 MPa, and SS316L at 200 and 350 MPa.

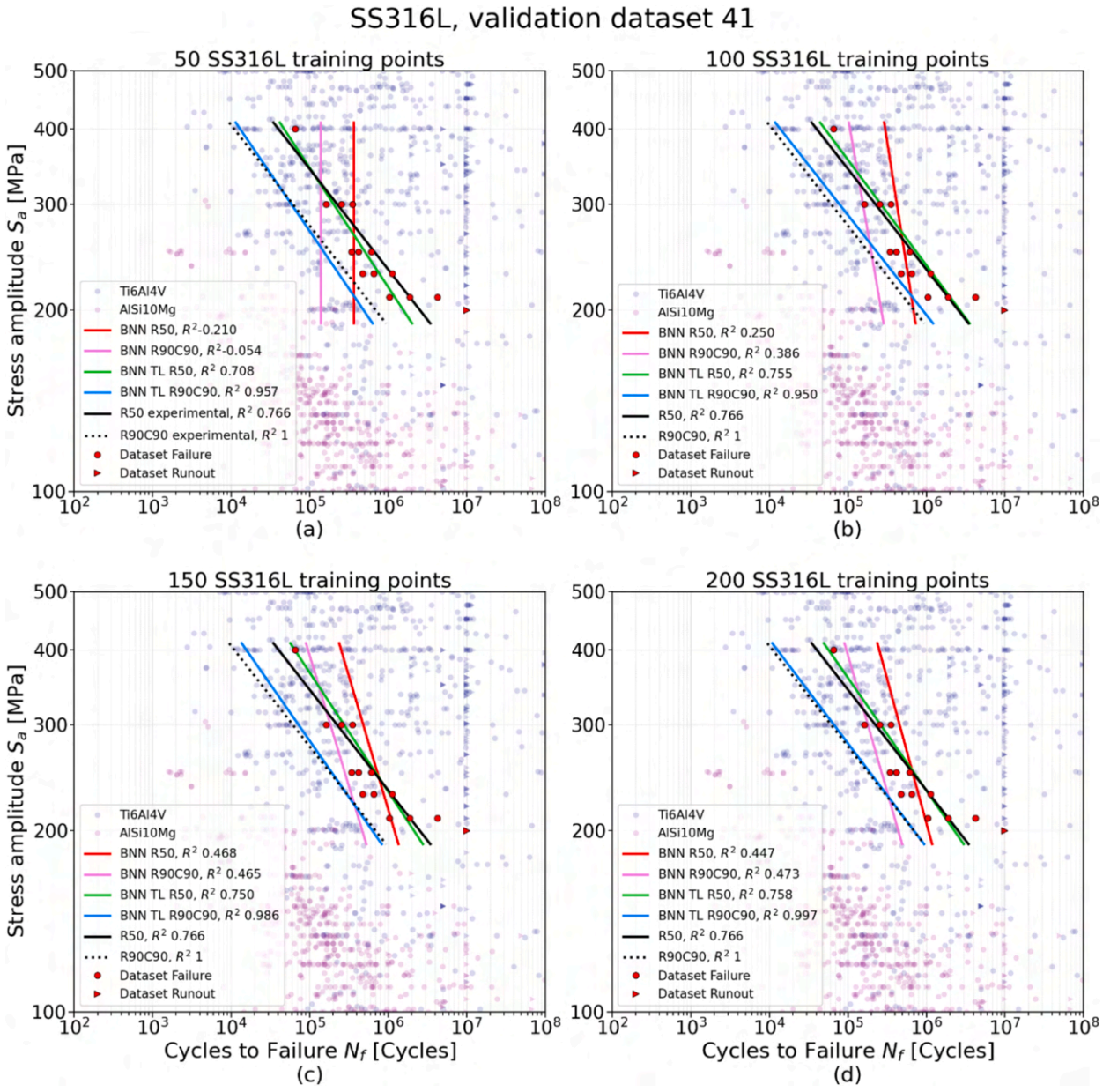


Fig. 12. PSN curves to assess the effectiveness of TL on SS316L from a BNN pretrained on AlSi10Mg (purple points) and Ti6Al4V (blue points). The external dataset 41 (red points and triangles) has been validated with combinations of 50 (a), 100 (b), 150 (c) and 200 (d) training points to output the R50 (red without TL and green with TL) and R90C90 life (magenta without TL and blue with TL) with and without TL. In solid black the experimental R50 line, while in dashed black the experimental R90C90 line.

Fig. 14 illustrates the overall influence of the process parameters on the fatigue life of each alloy, and it highlights the capabilities of the BNN to deliver probabilistic confidence envelopes, as in [42]. The influence of individual process parameters is analysed per alloy and visualised in columns (Ti6Al4V: Fig. 14a, d, g, j and m; AlSi10Mg: Fig. 14b, e, h, k, and n; SS316L: Fig. 14c, f, i, l and o), whereas each row corresponds to a different process parameter: building orientation (ϑ), laser power (P), scan speed (v), hatch distance (h), and layer thickness (t). Overall, it can be observed that in the majority of the cases there is accordance between the alloys for the same process parameters. For ϑ, Ti6Al4V, AlSi10Mg, and SS316L show similar trends at both S_a levels, with the horizontal configuration showing the highest fatigue resistance, in agreement with previous studies [54–57]. Higher values of P improve the fatigue life of both

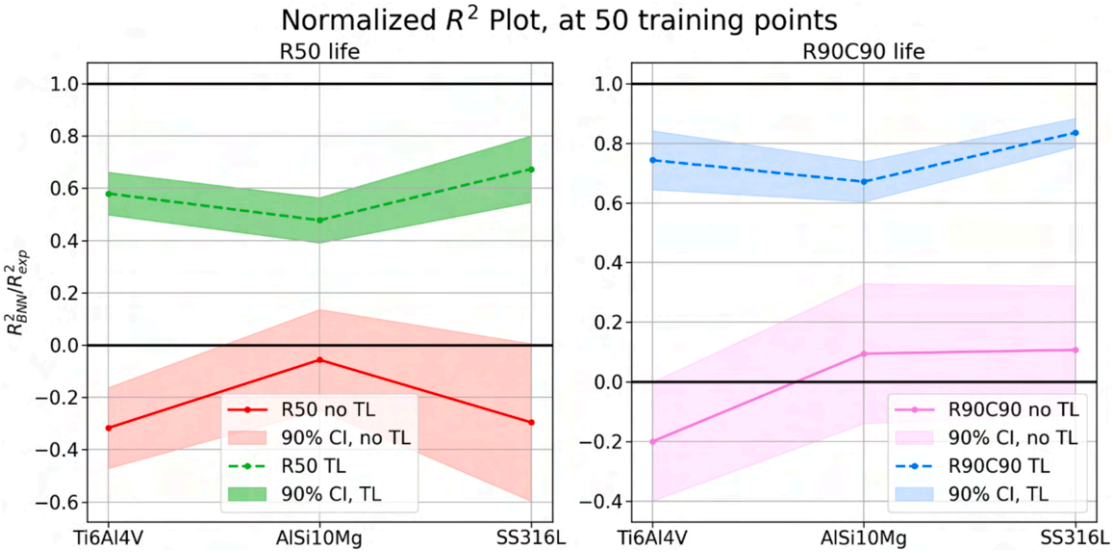


Fig. 13. Effectiveness of TL at 50 training points evaluated with the normalized R^2 score averaged on all external validation datasets for all alloys. Each point is averaged with respect to 14 external datasets R^2_{norm} scores for Ti6Al4V, 16 for AlSi10Mg and 11 for SS316L. The 90% confidence interval of the mean is also reported.

Table 2
Process parameters most recurrent values to which the evaluation database has been set to per alloy.

Alloy	ϑ [°]	P [W]	v [mm/s]	h [μm]	t [μm]
Ti6Al4V	90	280	1200	100	30
AlSi10Mg	90	370	1300	130	30
SS316L	90	275	1000	100	30

Ti6Al4V and AlSi10Mg. However, the BNN indicates that the predictions are less reliable at high values of P, as in that region the prediction uncertainty envelope gets larger. At the higher S_a levels, the model shows a sweet spot of 225–275 W for Ti6Al4V, and around 350 W for AlSi10Mg (Fig. 14d-e). In the case of SS316L, increasing P leads to a reduced fatigue strength, as observed in [35]. Analogue findings are reported in the literature, where the optimal values of P discussed above showed a reduction of the final porosity for AlSi10Mg, SS316L and Ti6Al4V [17,58,59]. For v, a sweet spot can be noticed here as well, especially for Ti6Al4V in the 800–1000 mm/s range. AlSi10Mg exhibits a similar behavior up to about 1500 mm/s. Higher N_f values occur at lower v, where the BNN indicates increased uncertainty. Notably, the BNN proves to be effective in signalling prediction reliability, as the widening of the uncertainty envelope directly reflects reduced confidence. For SS316L, no significant differences are found within v, though local peaks are found near 1500 mm/s. The findings align with the literature. Refs. [59,60] report low porosity at $v \approx 1250$ mm/s, while ref. [17] shows trends consistent with Fig. 14g for Ti6Al4V, with low porosities near 1000 mm/s. For SS316L, ref. [58] has shown that v between 800 and 1200 mm/s gives high relative density (ρ_{rel}), with a maximum at 1200 mm/s, whereas exceeding 1250 mm/s causes a drastic decrease of ρ_{rel}. Similarly, ref. [61] confirmed that $v \approx 1200$ mm/s leads to the highest ρ_{rel}. For h, the results are similar for the three alloys: a peak of N_f is observed in the 110–120 μm range. For the SS316L, this behavior is more evident at 200 MPa, while a larger uncertainty dominates at 350 MPa. The results are in agreement with the experimental evidence shown in [17,61,62]. Similar consistencies among the three alloys can be observed for t. Low values of t lead to a better response, with local peaks around $t \approx 35$–40 μm. The trends are in agreement with the experimental evidence reported in [17] and [58], where low values of t yield a lower porosity. All these results are in sound agreement with the experimental evidence, proving the effectiveness of the BNN in modelling the influences of the processing parameters on the fatigue response. It must be highlighted that the behaviors shown in Fig. 14 may differ if the reference configuration of Table 2 is changed.

5.2. Process parameters influence inference with TL

This section evaluates whether TL enables the newly assessed material (alloy A) to correctly infer the influence of process parameters on N_f from the other two alloys (B and C) under limited data conditions. The training and data selection procedures follow those described in Section 3.3, with the only difference being the use of 50 training data points and 10 random combinations of training subsets. Process parameters are plotted against N_f normalized with respect to the maximum value, and are evaluated for all three alloys both with TL (Fig. 15 green) and without TL (Fig. 15 red), and compared with the reference influence estimated by the BNN trained on

the full database of each alloy (Fig. 15 black), corresponding to the mean curves of Fig. 14. This reference serves to assess TL's ability to reproduce the correct parameter–life relationships. One S_a level is considered per alloy: 300 MPa for Ti6Al4V, 100 MPa for AlSi10Mg, and 200 MPa for SS316L. As in Section 4, the curves with and without TL are averaged over ten evaluations to reduce random effects, using identical dataset combinations in both cases. This constitutes a stringent test, since the pre-trained BNN has never seen data from the target material and is trained and fine-tuned using only 50 samples. Nevertheless, as shown in Fig. 15, TL successfully infers the parameter–life relationships for all three alloys. The case without TL (red) fails to follow the reference behaviour (black), while TL (green) reproduces the same trends, overlapping the reference almost perfectly for most of the parameter range. A mild overestimation or underestimation of the normalized N_f is sometimes present for a small portion of the parameter range. Despite these small discrepancies – attributable to differences in intrinsic material response at the same S_a – the optimal parameter ranges are correctly identified. As an example, in Fig. 15a, v evaluated on Ti6Al4V shows a reference optimal v range of 750–1000 mm/s. With TL the optimal range is correctly estimated with a v giving a high life at 1000 mm/s, whereas the case without TL completely struggles to follow the reference, giving an optimal v of 200 mm/s. Similarly, in Fig. 15b the optimal reference h value for Ti6Al4V is close to 125 μm, and is correctly predicted by TL, with its optimal value equal to 135 μm, whereas without TL the optimal h is missed with an estimate of 180 μm. The same holds for h for AlSi10Mg (Fig. 15e) in which TL not only correctly estimated the optimal h value (110

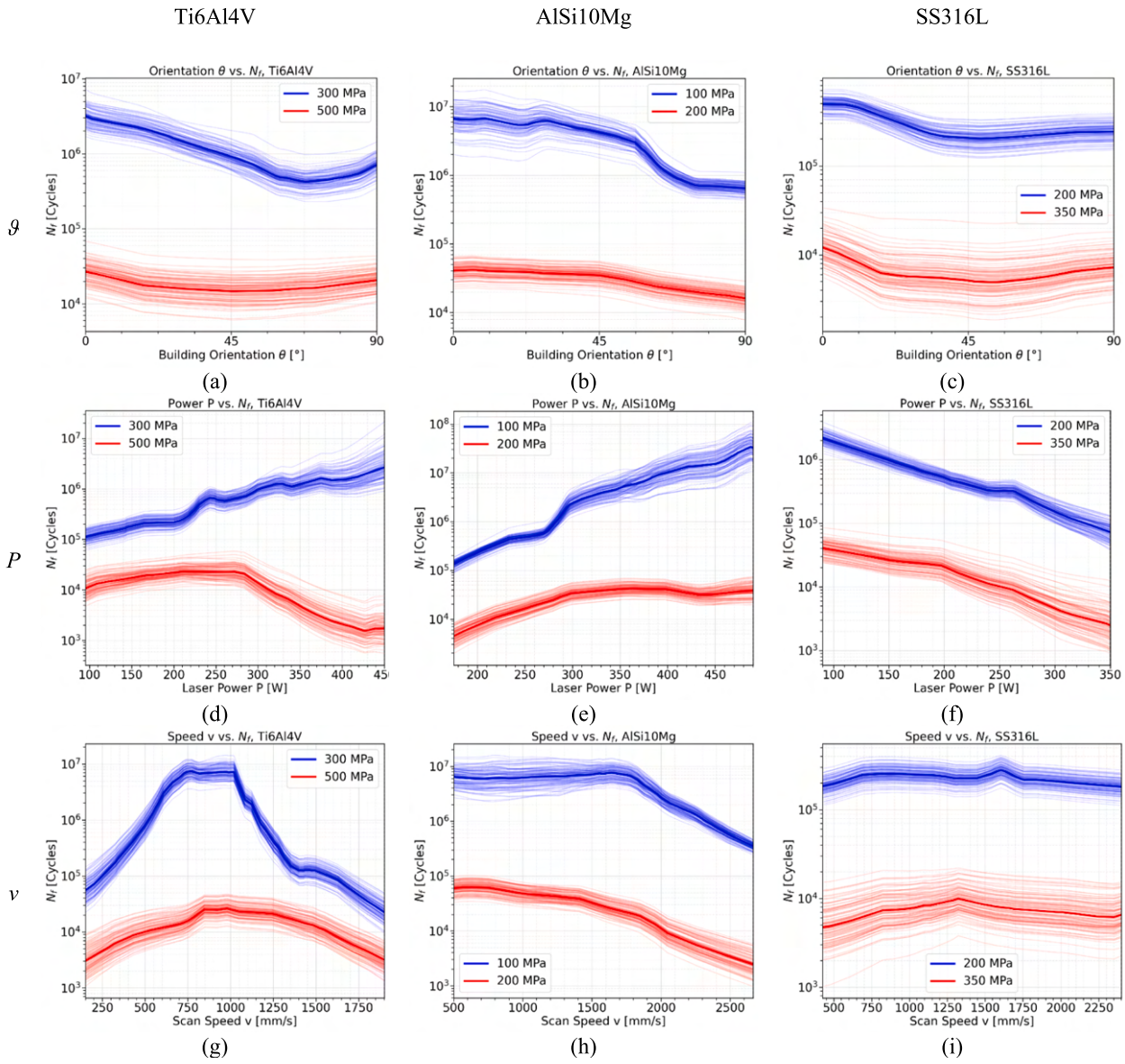


Fig. 14. Process parameters influence on the fatigue life, for Ti6Al4V (a, d, g, j and m), AlSi10Mg (b, e, h, k, and n) and SS316L (c, f, i, l and o). The influence on the fatigue response is analysed with respect to the building orientation ϑ (a, b and c), the laser power P (d, e and f), the scan speed v (g, h and i), the hatch distance h (j, k and l) and the layer thickness t (m, n and o).

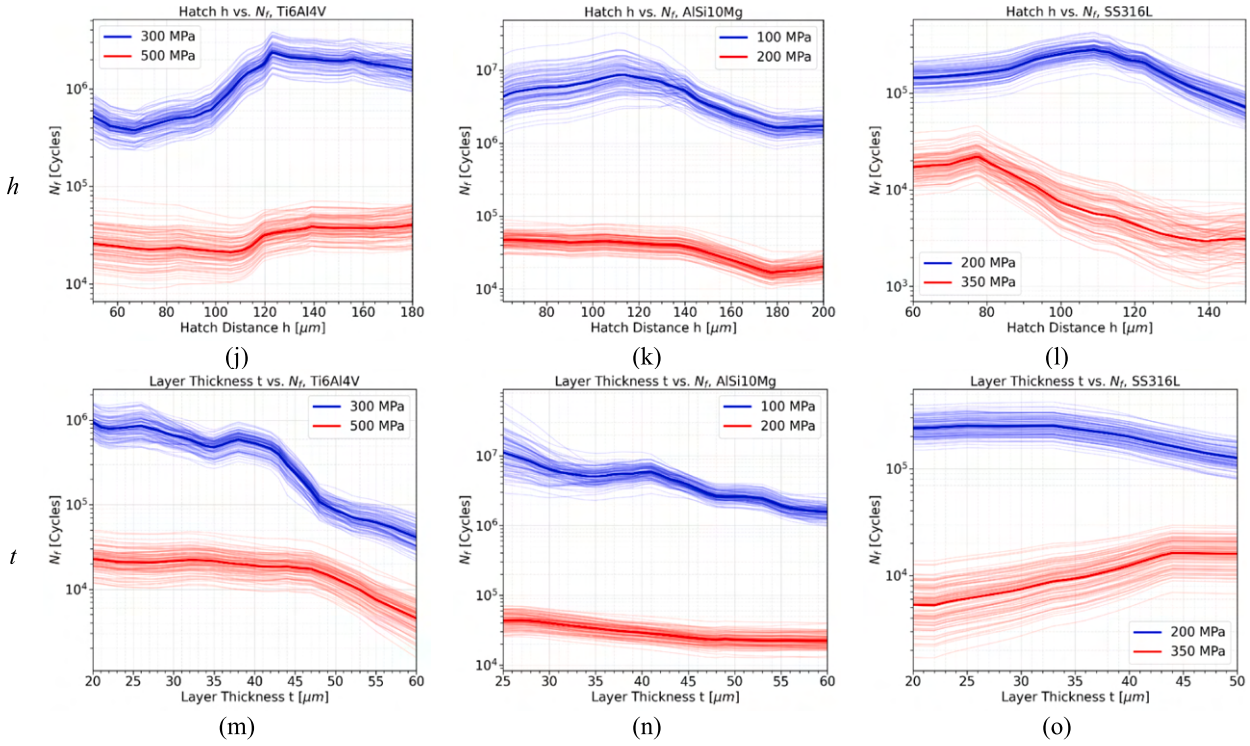


Fig. 14. (*continued*).

μm), but also correctly represents the overall behaviour by following the reference line with good accuracy, whereas standard training completely fails. In Fig. 15d, v is studied for AlSi10Mg, and the case with TL correctly estimates the reference line, especially the optimal v range plateau from 500 to 1700 mm/s and its suboptimal drop after it. On the other hand, the case without TL correctly estimates only its small peak at 1700 mm/s while incorrectly predicting as worse the portion below it up to 500 mm/s. When it comes to ϑ, P and t for SS316L (Fig. 15f-h), the case with and without TL both guess the optimal and suboptimal parameters value, however the case with TL shows superior accuracy as its behaviour is closer to the reference line as opposed to the case without TL. Overall, TL effectively transfers knowledge across different alloys, enabling accurate prediction of fatigue life and process parameter influence even under severe data scarcity.

TL significantly improves the prediction capabilities of the BNNs, as opposed to the case without TL, confirming its effectiveness under data-scarce scenarios. By leveraging pre-trained models and extensive literature data, TL improves both accuracy and reliability of the predictions.

6. Conclusions

The present work presents an approach to improve fatigue life prediction and design against fatigue failures under data scarce conditions, via transfer learning (TL) algorithms for additively manufactured (AMed) metallic alloys, allowing to save economical and temporal resources. TL transfers knowledge from a Bayesian neural network (BNN) pre-trained on alloys with larger datasets to improve accuracy when training data are limited.

TL was applied to Ti6Al4V (1106 points), AlSi10Mg (874 points), and SS316L (518 points), with data collected from more than 70 literature sources. Data scarcity was simulated for each alloy on rotation by subdividing its full database into smaller subsets of 50, 100, 150 and 200 data points. The performance of TL was assessed on external experimental validation datasets, not considered during training, by comparing the probabilistic stress life (PSN) curves (R50 and R90C90) and R^2 accuracy scores with and without TL.

The key findings can be summarized as follows:

- TL enhances prediction accuracy for all alloys, remarkably improving the R^2 score and the agreement of PSN curves with experimental data, regardless of the training database size.
- TL remains effective even with as few as 50 data points, yielding higher R^2 scores than models trained without TL. The R^2 score saturates quickly, indicating that expanding the training dataset beyond this size does not significantly increase the R^2 score.
- Moreover, the positive effect of TL is supported by the absence of overlap between the 90% confidence intervals of the means of the normalized R^2 scores for all alloys, suggesting that the observed difference is also statistically significant.

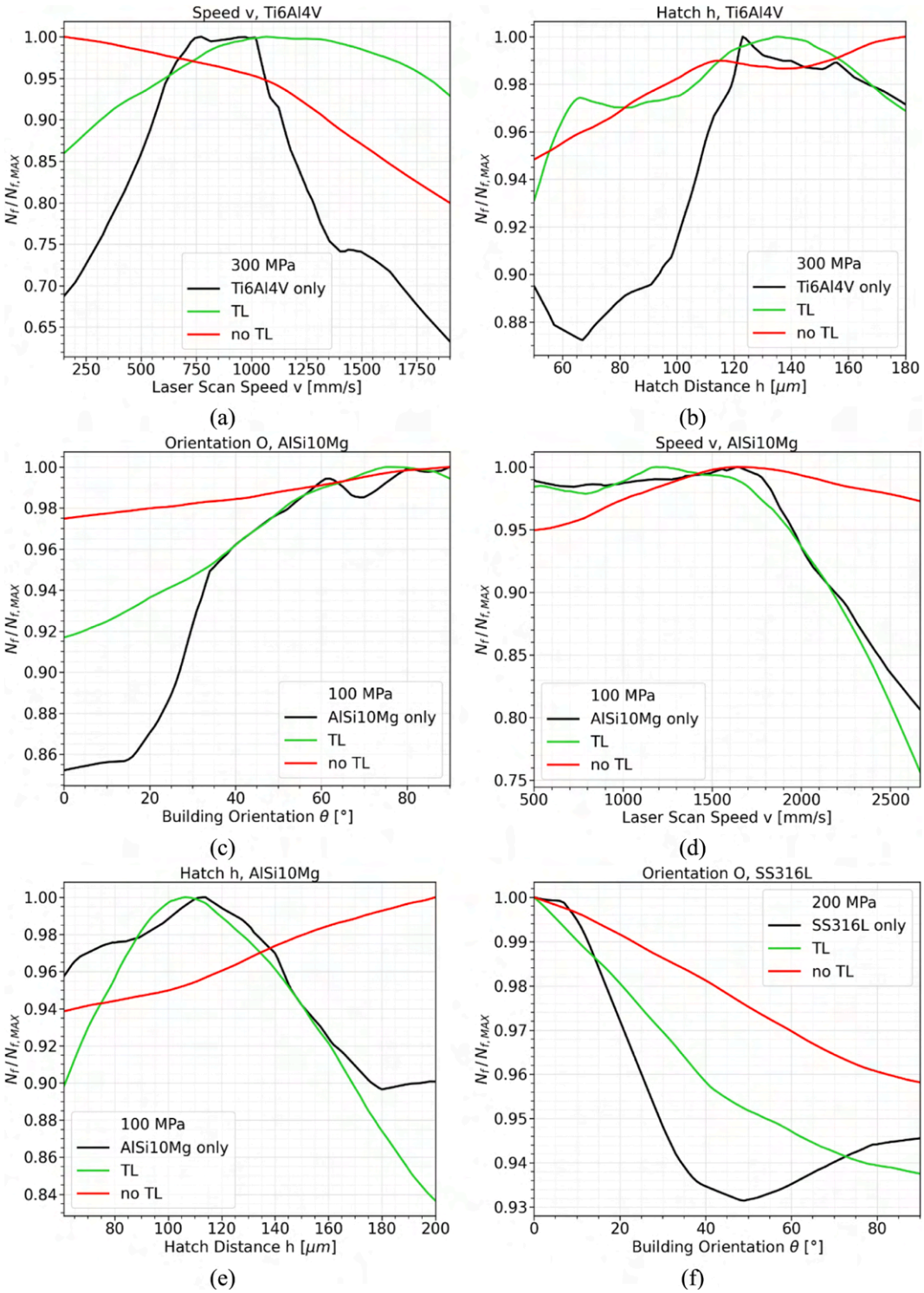


Fig. 15. TL process parameters influence inference for Ti6Al4V, AlSi10Mg and SS316L. The alloys have been evaluated at respectively 300, 100 and 200 MPa. On the x-axis the studied parameter, while on the y-axis N_f normalized with respect to the maximum. In black the process parameters evaluated with a BNN trained on the entire database of the evaluated alloy alone. In green the process parameters evaluated on a BNN trained with 10 different training combinations of 50 datapoints with TL, while in red the same but without TL.

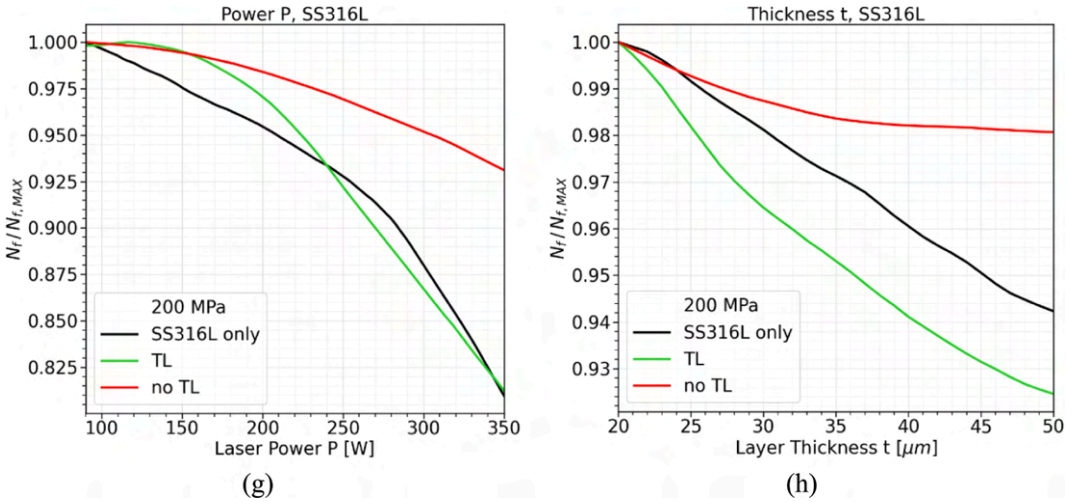


Fig. 15. (*continued*).

- SS316L benefits more from TL as its position in the stress-life (SN) diagram is between those of Ti6Al4V and AlSi10Mg, from which TL is performed. Conversely, the improvement for AlSi10Mg is smaller, as its external datasets lie way below those of the SS316L and Ti6Al4V, from which TL is performed.
- The effectiveness of TL depends on the relative location on the SN diagram of the studied alloy with respect to the alloys from which TL is performed.
- TL successfully captures the influence of process parameters on fatigue performance when training data is scarce, reproducing trends consistent with a BNN trained on the complete database, effectively improving the inference capabilities of the data-scarce BNNs over the process parameters influence.

In conclusion, TL offers a robust strategy for fatigue life prediction with limited data. By appropriately combining data normalization, data pre-processing, and adapting the pre-trained models through loading, freezing, and finetuning, TL significantly enhances the predictive capabilities, reliability, and generalization to mitigate fatigue failures. These techniques accelerate model training while reducing experimental and computational costs, paving the way for more efficient and trustworthy fatigue assessment of AM alloys with machine learning.

CRediT authorship contribution statement

Alessio Centola: Writing – original draft, Visualization, Validation, Software, Methodology, Investigation, Data curation, Conceptualization. **Alberto Ciampaglia:** Writing – review & editing, Validation, Supervision, Investigation, Conceptualization. **Davide Salvatore Paolino:** Writing – review & editing, Supervision, Project administration, Conceptualization. **Andrea Tridello:** Writing – review & editing, Supervision, Project administration, Formal analysis, Conceptualization.

Funding

This research did not receive any specific grant from funding agencies in the public, commercial, or not-for-profit sectors.

Declaration of competing interest

The Authors declare that they have no known competing financial interests or personal relationships that could have appeared to influence the work reported in this paper.

Appendix A:. Multi-alloy training database

The appendix reports the entire multi-alloy training database (Table A), with indexing and input features divided by alloy, article and dataset. The output labels such as S_a, N_f and R_f, have not been reported to keep Table A as concise as possible. The training data has been collected from 71 trusted literature sources, resulting in 222 datasets and 2498 points: 1106 points from 88 datasets from 32 articles for Ti6Al4V, 874 points from 83 datasets from 22 articles for AlSi10Mg and 518 points from 51 datasets from 17 articles for SS316L. Table A contains additional references [63–129] that are not cited elsewhere in the main body of the article. For further details about the input features and output labels, the reader is referred to Section 2.1.

Table A
Indexing and input features of the full multi alloy training database for Ti6Al4V, AlSi10Mg and SS316L. S_a, N_f and R_f have not been reported to keep this table as concise as possible.

Indexing						Process Parameters					Risk Volume	Thermal Traetments						Surface Treatments											
Overall Article Code	Overall Dataset Code	Ref	Material Article Code	Material Dataset Code	Material	N° Specimens	Orientation ϑ [°]	Laser Power P [W]	Scan Speed v [mm/s]	Hatch Distance h [µm]	Layer Thickness t [µm]	Risk Volume V_{risk} [mm³]	TT_Ann	T_Ann	dt_Ann	TT_HIP	T_HIP	P_HIP	dt_HIP	ST_Mac	ST_Pol	ST_Grind	ST_SB	ST_SP	ST_LSP	ST_FSP	ST_VF	ST_SMAT	ST_Nitr	ST_DN	ST_EDM	ST_EP
1	0	[17]	1	0	Ti6Al4V	12	90	120	1200	70	30	45.89	1	600	2	0	20	1	0	0	1	0	0	0	0	0	0	0	0	0	0
1	1		1	1		17	90	120	1000	100	45	45.89	1	600	2	0	20	1	0	0	1	0	0	0	0	0	0	0	0	0	0
1	2		1	2		14	90	120	800	130	60	45.89	1	600	2	0	20	1	0	0	1	0	0	0	0	0	0	0	0	0	0
1	3		1	3		16	90	160	1000	130	30	45.89	1	600	2	0	20	1	0	0	1	0	0	0	0	0	0	0	0	0	0
1	4		1	4		17	90	160	800	70	45	45.89	1	600	2	0	20	1	0	0	1	0	0	0	0	0	0	0	0	0	0
1	5		1	5		13	90	160	1200	100	60	45.89	1	600	2	0	20	1	0	0	1	0	0	0	0	0	0	0	0	0	0
1	6		1	6		14	90	200	800	100	30	45.89	1	600	2	0	20	1	0	0	1	0	0	0	0	0	0	0	0	0	0
1	7		1	7		13	90	200	1200	130	45	45.89	1	600	2	0	20	1	0	0	1	0	0	0	0	0	0	0	0	0	0
1	8		1	8		16	90	200	1000	70	60	45.89	1	600	2	0	20	1	0	0	1	0	0	0	0	0	0	0	0	0	0
1	9		1	9		19	90	160	1000	70	30	45.89	1	600	2	0	20	1	0	0	1	0	0	0	0	0	0	0	0	0	0
2	10	[63]	2	10		16	90	175	710	120	30	45.60	1	800	2	0	20	1	0	1	0	0	0	0	0	0	0	0	0	0	0
2	11		2	11		19	90	175	710	120	30	50.62	1	800	2	0	20	1	0	1	1	0	0	0	0	0	0	0	0	0	0
2	12		2	12		16	90	175	710	120	30	50.62	0	20	0	1	920	1000	2	1	1	0	0	0	0	0	0	0	0	0	0
3	13	[64]	3	13		21	90	280	1200	140	30	149.60	1	500	2	0	20	1	0	0	1	0	0	0	0	0	0	0	0	0	0
4	14	[65]	4	14		5	90	200	1000	100	50	769.69	0	20	0	0	20	1	0	1	0	0	0	0	0	0	0	0	0	0	0
4	15		4	15		3	90	200	1000	100	50	769.69	0	20	0	1	930	1300	3	1	0	0	0	0	0	0	0	0	0	0	0
5	16	[66]	5	16		15	90	200	1250	80	30	150.43	1	820	1.5	0	20	1	0	0	0	0	0	0	0	0	0	0	0	0	0
6	17	[67]	6	17		10	0	190	1000	65	30	59.36	1	955	2	0	20	1	0	0	1	0	0	0	0	0	0	0	0	0	0
6	18		6	18		10	0	190	1000	65	30	59.36	0	20	0	0	20	1	0	0	1	0	0	0	1	0	0	0	0	0	0
7	19	[68]	7	19		17	90	360	1200	100	60	23.58	1	710	2	1	920	1000	2	0	1	1	0	0	0	0	0	0	0	0	0
7	20		7	20		14	90	360	1200	100	60	7.72	1	710	2	1	920	1000	2	0	1	1	0	0	0	0	0	0	0	0	0
8	21	[69]	8	21		12	45	170	1250	100	30	149.60	1	650	3	0	20	1	0	0	0	0	0	0	0	0	0	0	0	0	0
8	22		8	22		12	45	170	1250	100	30	149.60	1	650	3	0	20	1	0	0	1	0	0	0	0	0	0	0	0	0	0
8	23		8	23		15	45	170	1250	100	30	149.60	1	650	3	0	20	1	0	0	0	0	0	1	0	0	0	0	0	0	0
9	24	[70]	9	24		12	90	120	960	100	30	63.62	0	20	0	0	20	1	0	1	1	0	1	0	0	0	0	0	0	0	0
9	25		9	25		11	90	120	540	100	30	63.62	0	20	0	0	20	1	0	1	1	0	1	0	0	0	0	0	0	0	0

(*continued on next page*)

Table A (*continued*)

9	26		9	26		11	90	1200	400	1000	30	63.62	0	20	0	0	20	1	0	1	1	0	1	0	0	0	0	0	0	0	0	0	0
9	27		9	27		12	90	1200	1260	1000	30	63.62	0	20	0	0	20	1	0	1	1	0	1	0	0	0	0	0	0	0	0	0	0
9	28		9	28		9	90	1200	1500	1000	30	63.62	0	20	0	0	20	1	0	1	1	0	1	0	0	0	0	0	0	0	0	0	0
10	29	[71]	10	29		9	90	4000	150	1200	60	133.78	0	20	0	0	20	1	0	1	0	0	0	0	0	0	0	0	0	0	0	0	0	0
10	30		10	30		22	90	4000	150	1200	60	133.78	0	20	0	1	8500	2000	2	1	0	0	0	0	0	0	0	0	0	0	0	0	0	0
11	31	[72]	11	31		20	90	1700	1200	1000	30	471.24	0	20	0	0	20	1	0	0	0	0	0	0	0	0	0	0	0	0	0	0	0	0
12	32	[73]	12	32		18	90	2000	1250	800	30	149.60	0	20	0	1	9200	10200	2	0	0	0	0	0	0	0	0	0	0	0	0	0	0	0
12	33		12	33		20	90	2000	1250	800	30	149.60	0	20	0	1	9200	10200	2	1	1	0	0	0	0	0	0	0	0	0	0	0	0	0
12	34		12	34		12	90	2000	1250	800	30	149.60	1	8200	1.5	0	20	1	0	1	1	0	0	0	0	0	0	0	0	0	0	0	0	0
13	35	[53]	13	35		16	90	2800	1200	1400	30	339.29	1	9000	1	0	20	1	0	0	0	0	0	0	0	0	0	0	0	0	0	0	0	0
13	36		13	36		17	90	2800	1200	1400	30	339.29	1	9000	1	0	20	1	0	0	0	0	0	0	0	0	0	0	0	0	0	0	0	0
13	37		13	37		20	90	2800	1200	1400	30	235.62	1	9000	1	0	20	1	0	1	1	0	0	0	0	0	0	0	0	0	0	0	0	0
13	38		13	38		20	90	2800	1200	1400	30	235.62	1	9000	1	0	20	1	0	1	1	0	0	0	0	0	0	0	0	0	0	0	0	0
14	39	[74]	14	39		11	90	2800	1200	500	30	129.53	0	20	0	0	20	1	0	0	0	0	0	0	0	0	0	0	0	0	0	0	0	0
14	40		14	40		11	90	2800	1200	500	30	129.53	0	20	0	1	9000	12000	2	1	0	0	0	0	0	0	0	0	0	0	0	0	0	0
14	41		14	41		10	90	2800	1200	500	30	129.53	0	20	0	1	9000	12000	2	1	0	0	0	0	0	0	0	1	0	0	0	0	0	0
15	42	[75]	15	42		11	90	2800	1200	1400	30	21.74	0	20	0	0	20	1	0	1	1	0	0	0	0	0	0	0	0	0	0	0	0	0
15	43		15	43		3	90	2800	1200	1400	30	21.74	1	9200	0.5	0	20	1	0	1	1	0	0	0	0	0	0	0	0	0	0	0	0	0
15	44		15	44		6	90	2800	1200	1400	30	21.74	1	9200	0.5	0	20	1	0	1	0	0	0	1	0	0	0	0	0	0	0	0	0	0
15	45		15	45		12	90	2800	1200	1400	30	21.74	0	20	0	0	20	1	0	1	1	0	0	0	0	0	0	0	0	0	0	0	0	0
15	46		15	46		7	90	2800	1200	1400	30	21.74	1	9200	0.5	0	20	1	0	1	1	0	0	0	0	0	0	0	0	0	0	0	0	0
15	47		15	47		7	90	2800	1200	1400	30	21.74	1	9200	0.5	0	20	1	0	1	0	0	0	1	0	0	0	0	0	0	0	0	0	0
15	48		15	48		8	90	3400	1250	1200	60	21.74	0	20	0	0	20	1	0	1	1	0	0	0	0	0	0	0	0	0	0	0	0	0
15	49		15	49		4	90	3400	1250	1200	60	21.74	1	9200	0.5	0	20	1	0	1	1	0	0	0	0	0	0	0	0	0	0	0	0	0
15	50		15	50		6	90	3400	1250	1200	60	21.74	1	9200	0.5	0	20	1	0	1	0	0	0	1	0	0	0	0	0	0	0	0	0	0
15	51		15	51		9	90	3400	1250	1200	60	21.74	0	20	0	0	20	1	0	1	1	0	0	0	0	0	0	0	0	0	0	0	0	0
15	52		15	52		4	90	3400	1250	1200	60	21.74	1	9200	0.5	0	20	1	0	1	1	0	0	0	0	0	0	0	0	0	0	0	0	0
15	53		15	53		5	90	3400	1250	1200	60	21.74	1	9200	0.5	0	20	1	0	1	0	0	0	1	0	0	0	0	0	0	0	0	0	0
16	54	[76]	16	54		12	90	2800	1200	1400	30	1200.00	1	6500	3	0	20	1	0	0	0	0	0	0	0	0	0	0	0	0	0	0	0	0
16	55		16	55		7	90	2800	1200	1400	30	1200.00	1	6500	3	0	20	1	0	0	0	0	0	0	1	0	0	0	0	0	0	0	0	0
17	56	[77]	17	56		22	0	2850	1200	1400	30	63.66	1	6500	3	0	20	1	0	1	0	0	0	0	0	0	0	0	0	0	0	0	0	0
18	57	[78]	18	57		9	90	2800	1200	1400	30	294.00	1	7000	1	0	20	1	0	0	0	0	0	0	0	0	0	0	0	0	0	0	0	0

(*continued on next page*)

Table A (*continued*)

18	58		18	58		9	90	2800	1200	140	30	294.00	1	700	1	0	20	1	0	0	1	0	0	0	0	0	0	0	0	0	0
19	59	[79]	19	59		13	90	3700	1250	90	60	239.46	1	650	2	0	20	1	0	0	0	0	0	0	0	0	0	0	0	0	0
19	60		19	60		9	90	3700	1250	90	60	239.46	1	650	2	0	20	1	0	1	1	0	0	0	0	0	0	0	0	0	0
20	61	[80]	20	61		7	0	2200	660	90	60	577.27	0	20	0	0	20	1	0	0	0	0	0	0	0	0	0	0	0	0	0
20	62		20	62		11	0	2200	660	90	60	577.27	1	850	2	0	20	1	0	0	0	0	0	0	0	0	0	0	0	0	0
21	63	[81]	21	63		9	0	95	300	80	25	1300.00	0	20	0	0	20	1	0	0	1	0	0	0	0	0	0	0	0	0	0
22	64	[82]	22	64		19	90	125	925	80	20	107.84	1	950	0.5	0	20	1	0	1	0	0	0	0	0	0	0	0	0	0	0
23	65	[83]	23	65		27	90	1700	1250	100	30	339.29	1	650	3	0	20	1	0	0	0	0	0	0	0	0	0	0	0	1	0
24	66	[84]	24	66		10	90	1750	710	125	30	199.12	0	20	0	0	20	1	0	1	0	0	0	0	0	0	0	0	0	0	0
24	67		24	67		10	0	1750	710	125	30	199.12	0	20	0	0	20	1	0	1	0	0	0	0	0	0	0	0	0	0	0
25	68	[85]	25	68		8	90	3000	1000	120	40	712.75	1	500	2	0	20	1	0	0	1	0	0	0	0	0	0	0	0	0	0
25	69		25	69		6	90	3000	1000	120	40	712.75	1	500	2	1	920	1000	2	0	1	0	0	0	0	0	0	0	0	0	0
25	70		25	70		6	90	3000	1000	120	40	712.75	1	920	2	0	20	1	0	0	1	0	0	0	0	0	0	0	0	0	0
25	71		25	71		6	90	3000	1000	120	40	712.75	1	550	4	0	20	1	0	0	1	0	0	0	0	0	0	0	0	0	0
26	72	[86]	26	72		17	90	4500	1200	150	50	31.94	1	850	2	0	20	1	0	1	0	0	0	0	0	0	0	0	0	0	0
26	73		26	73		20	45	4500	1200	150	50	31.94	1	850	2	0	20	1	0	1	0	0	0	0	0	0	0	0	0	0	0
26	74		26	74		22	0	4500	1200	150	50	31.94	1	850	2	0	20	1	0	1	0	0	0	0	0	0	0	0	0	0	0
27	75	[87]	27	75		20	90	1250	925	80	20	191.31	1	950	0.5	0	20	1	0	1	0	0	0	0	0	0	0	0	0	0	0
28	76	[88]	28	76		12	90	2800	1200	50	50	129.53	1	900	2	0	20	1	0	1	0	0	0	0	0	0	0	0	0	0	0
29	77	[89]	29	77		24	0	3500	1250	100	60	149.60	1	800	2	0	20	1	0	1	0	0	0	0	0	0	0	0	0	0	0
29	78		29	78		19	0	3500	1250	100	60	149.60	1	800	2	0	20	1	0	1	0	0	0	0	0	0	0	0	0	0	0
30	79	[90]	30	79		15	0	2000	200	180	50	10560.00	0	20	0	0	20	1	0	1	1	0	0	0	0	0	0	0	0	0	0
30	80		30	80		7	90	2000	200	180	50	10560.00	0	20	0	0	20	1	0	1	1	0	0	0	0	0	0	0	0	0	0
30	81		30	81		10	0	2000	200	180	50	10560.00	0	20	0	0	20	1	0	0	0	0	0	0	0	0	0	0	0	0	0
30	82		30	82		5	90	2000	200	180	50	10560.00	0	20	0	0	20	1	0	0	0	0	0	0	0	0	0	0	0	0	0
31	83	[91]	31	83		7	90	2000	1200	100	30	180.00	0	20	0	0	20	1	0	0	0	0	0	0	0	0	0	0	0	0	0
31	84		31	84		8	90	2000	1900	100	30	180.00	0	20	0	0	20	1	0	0	0	0	0	0	0	0	0	0	0	0	0
32	85	[92]	32	85		16	90	3400	1250	120	60	508.94	1	900	2	0	20	1	0	1	0	0	0	0	0	0	0	0	0	0	0
32	86		32	86		11	90	3400	1250	120	60	508.94	1	732	2	0	20	1	0	1	0	0	0	0	0	0	0	0	0	0	0
32	87		32	87		13	90	3400	1250	120	60	508.94	1	732	2	1	900	1000	2	1	0	0	0	0	0	0	0	0	0	0	0
33	88	[93]	1	0	AlSi10Mg	21	0	3000	2666.67	80	30	629.83	0	20	0	0	20	1	0	1	0	0	0	0	0	0	0	0	0	0	0
33	89		1	1		17	0	2000	1109.091	61	30	629.83	0	20	0	0	20	1	0	1	0	0	0	0	0	0	0	0	0	0	0
33	90		1	2		19	0	275	2000	80	30	629.83	0	20	0	0	20	1	0	1	0	0	0	0	0	0	0	0	0	0	0

(*continued on next page*)

Table A (*continued*)

34	91	[94]	2	3		10	0	250	500	150	50	149.60	1	165	7	0	20	1	0	1	0	0	0	0	0	0	0	0	0	0	0	0	0
34	92		2	4		10	90	250	500	150	50	149.60	1	165	7	0	20	1	0	1	0	0	0	0	0	0	0	0	0	0	0	0	0
34	93		2	5		9	45	250	500	150	50	149.60	1	165	7	0	20	1	0	1	0	0	0	0	0	0	0	0	0	0	0	0	0
34	94		2	6		7	0	250	500	150	50	149.60	0	20	0	0	20	1	0	1	0	0	0	0	0	0	0	0	0	0	0	0	0
34	95		2	7		11	0	250	500	150	50	149.60	1	165	7	0	20	1	0	1	0	0	0	0	0	0	0	0	0	0	0	0	0
34	96		2	8		10	90	250	500	150	50	149.60	0	20	0	0	20	1	0	1	0	0	0	0	0	0	0	0	0	0	0	0	0
34	97		2	9		8	90	250	500	150	50	149.60	1	165	7	0	20	1	0	1	0	0	0	0	0	0	0	0	0	0	0	0	0
34	98		2	10		9	45	250	500	150	50	149.60	0	20	0	0	20	1	0	1	0	0	0	0	0	0	0	0	0	0	0	0	0
34	99		2	11		11	45	250	500	150	50	149.60	1	165	7	0	20	1	0	1	0	0	0	0	0	0	0	0	0	0	0	0	0
35	100	[95]	3	12		18	90	350	1200	190	50	211.64	0	20	0	0	20	1	0	1	0	0	0	0	0	0	0	0	0	0	0	0	0
35	101		3	13		18	90	350	1200	190	50	379.42	0	20	0	0	20	1	0	1	0	0	0	0	0	0	0	0	0	0	0	0	0
36	102	[96]	4	14		10	90	400	1000	200	60	196.35	0	20	0	0	20	1	0	1	1	0	0	0	0	0	0	0	0	0	0	0	0
36	103		4	15		9	90	400	1000	200	60	196.35	0	20	0	0	20	1	0	1	0	0	0	0	0	0	0	0	0	0	0	0	0
36	104		4	16		15	90	400	1000	200	60	196.35	1	300	2	0	20	1	0	1	1	0	0	0	0	0	0	0	0	0	0	0	0
36	105		4	17		4	90	400	1000	200	60	196.35	1	300	2	1	250	1800	2	1	1	0	0	0	0	0	0	0	0	0	0	0	0
36	106		4	18		4	90	400	1000	200	60	196.35	1	300	2	1	250	1800	2	1	0	0	0	0	0	0	0	0	0	0	0	0	0
36	107		4	19		4	90	400	1000	200	60	196.35	1	300	2	1	250	1800	2	0	0	0	0	0	0	0	0	0	0	0	0	0	0
36	108		4	20		3	90	400	1000	200	60	196.35	1	300	2	1	500	1800	2	1	1	0	0	0	0	0	0	0	0	0	0	0	0
36	109		4	21		3	90	400	1000	200	60	196.35	1	300	2	1	500	1800	2	1	0	0	0	0	0	0	0	0	0	0	0	0	0
36	110		4	22		3	90	400	1000	200	60	196.35	1	300	2	1	500	1800	2	0	0	0	0	0	0	0	0	0	0	0	0	0	0
37	111	[97]	5	23		14	90	400	1000	200	60	196.35	1	300	2	0	20	1	0	1	0	0	0	1	0	0	0	0	0	0	0	0	0
37	112		5	24		17	90	400	1000	200	60	196.35	1	300	2	0	20	1	0	1	1	0	0	1	0	0	0	0	0	0	0	0	0
38	113	[98]	6	25		14	90	350	1650	130	30	299.24	0	20	0	0	20	1	0	1	1	0	0	0	0	0	0	0	0	0	0	0	0
38	114		6	26		6	90	350	1650	130	30	299.24	1	500	1	0	20	1	0	0	1	0	0	0	0	0	0	0	0	0	0	0	0
38	115		6	27		17	90	350	1650	130	30	299.24	1	300	2	0	20	1	0	1	1	0	0	0	0	0	0	0	0	0	0	0	0
38	116		6	28		20	0	350	1650	130	30	299.24	1	300	2	0	20	1	0	1	1	0	0	0	0	0	0	0	0	0	0	0	0
39	117	[99]	7	29		9	90	390	1300	190	30	13.54	0	20	0	0	20	1	0	0	1	0	0	0	0	0	0	0	0	0	0	0	0
39	118		7	30		6	90	390	1300	190	30	13.54	1	200	8	1	497	1000	2	0	1	0	0	0	0	0	0	0	0	0	0	0	0
39	119		7	31		8	90	390	1300	190	30	13.54	0	20	0	1	350	30000	2	0	1	0	0	0	0	0	0	0	0	0	0	0	0
40	120	[100]	8	32		26	90	370	1300	190	30	346.84	0	20	0	0	20	1	0	1	0	0	0	0	0	0	0	0	0	0	0	0	0
40	121		8	33		10	90	370	1300	190	30	346.84	1	160	7	1	500	100	2	1	0	0	0	0	0	0	0	0	0	0	0	0	0

(*continued on next page*)

Table A (*continued*)

40	122		8	34		13	90	3700	1300	190	30	346.84	1	300	2	0	20	1	0	1	0	0	0	0	0	0	0	0	0	0	0	0	0
41	123	[101]	9	35		4	90	4900	2000	100	40	570.20	0	20	0	0	20	1	0	1	0	0	0	0	0	0	0	0	0	0	0	0	0	0
41	124		9	36		3	90	4900	2000	100	40	570.20	1	300	2	0	20	1	0	1	0	0	0	0	0	0	0	0	0	0	0	0	0	0
41	125		9	37		5	90	4900	2000	100	40	570.20	1	530	1	0	20	1	0	1	0	0	0	0	0	0	0	0	0	0	0	0	0	0
41	126		9	38		3	90	4900	2000	100	40	570.20	1	170	12	0	20	1	0	1	0	0	0	0	0	0	0	0	0	0	0	0	0	0
42	127	[102]	10	39		7	90	3700	1300	130	30	294.52	1	300	2	0	20	1	0	0	0	0	0	0	0	0	0	0	0	0	0	0	0	0
42	128		10	40		7	90	3700	1300	130	30	294.52	1	270	1.5	0	20	1	0	0	0	0	0	0	0	0	0	0	0	0	0	0	0	0
42	129		10	41		6	90	3700	1300	130	30	294.52	1	300	2	0	20	1	0	1	0	0	0	0	0	0	0	0	0	0	0	0	0	0
42	130		10	42		8	90	3700	1300	130	30	294.52	1	270	1.5	0	20	1	0	1	0	0	0	0	0	0	0	0	0	0	0	0	0	0
43	131	[103]	11	43		19	0	3800	1350	145	50	294.52	1	300	2	0	20	1	0	0	1	1	0	0	0	0	0	0	0	0	0	0	0	0
43	132		11	44		22	90	3800	1350	145	50	294.52	1	300	2	0	20	1	0	0	1	1	0	0	0	0	0	0	0	0	0	0	0	0
44	133	[104]	12	45		14	90	3500	1650	130	50	196.35	1	200	4	0	20	1	0	0	0	0	0	0	0	0	0	0	0	0	0	0	0	0
44	134		12	46		12	90	3500	1650	130	50	196.35	1	200	4	0	20	1	0	1	1	0	0	0	0	0	0	0	0	0	0	0	0	0
45	135	[105]	13	47		6	0	3300	1700	150	30	78.95	1	270	2	0	20	1	0	1	1	0	0	0	0	0	0	0	0	0	0	0	0	0
45	136		13	48		6	45	3300	1700	150	30	78.95	1	270	2	0	20	1	0	1	1	0	0	0	0	0	0	0	0	0	0	0	0	0
45	137		13	49		8	90	3300	1700	150	30	78.95	1	270	2	0	20	1	0	1	1	0	0	0	0	0	0	0	0	0	0	0	0	0
46	138	[106]	14	50		6	90	2000	570	80	25	211.00	0	20	0	0	20	1	0	0	0	0	0	0	0	0	0	0	0	0	0	0	0	0
46	139		14	51		8	90	2000	570	80	25	211.00	0	20	0	0	20	1	0	1	0	0	0	0	0	0	0	0	0	0	0	0	0	0
46	140		14	52		5	90	2000	570	80	25	211.00	1	160	6	0	20	1	0	0	0	0	0	0	0	0	0	0	0	0	0	0	0	0
46	141		14	53		4	90	2000	570	80	25	211.00	1	160	6	0	20	1	0	1	0	0	0	0	0	0	0	0	0	0	0	0	0	0
47	142	[107]	15	54		20	90	4000	1000	200	50	5.20	1	520	2	0	20	1	0	1	1	0	0	0	0	0	0	0	0	0	0	0	0	0
47	143		15	55		22	45	4000	1000	200	50	5.20	1	520	2	0	20	1	0	1	1	0	0	0	0	0	0	0	0	0	0	0	0	0
47	144		15	56		19	0	4000	1000	200	50	5.20	1	520	2	0	20	1	0	1	1	0	0	0	0	0	0	0	0	0	0	0	0	0
48	145	[108]	16	57		22	90	3700	1300	190	30	452.39	0	20	0	0	20	1	0	0	0	0	0	0	0	0	0	0	0	0	0	0	0	0
48	146		16	58		18	90	3700	1300	190	30	452.39	0	20	0	0	20	1	0	1	0	0	0	0	0	0	0	0	0	0	0	0	0	0
49	147	[109]	17	59		6	0	3700	1300	190	30	13.54	0	20	0	0	20	1	0	1	1	0	0	0	0	0	0	0	0	0	0	0	0	0
49	148		17	60		13	0	3700	1300	190	30	13.54	1	300	2	0	20	1	0	1	1	0	0	0	0	0	0	0	0	0	0	0	0	0
49	149		17	61		13	0	3700	1300	190	30	13.54	0	20	0	0	20	1	0	1	1	0	0	0	0	1	0	0	0	0	0	0	0	0
50	150	[110]	18	62		7	90	2500	800	130	30	288.00	0	20	0	0	20	1	0	0	0	0	0	0	0	0	0	0	0	0	0	0	0	0
50	151		18	63		7	90	2500	800	130	30	288.00	1	300	2	0	20	1	0	0	0	0	0	0	0	0	0	0	0	0	0	0	0	0
50	152		18	64		9	90	2500	800	130	30	288.00	1	282	4	0	20	1	0	0	0	0	0	0	0	0	0	0	0	0	0	0	0	0
50	153		18	65		6	90	2500	800	130	30	288.00	1	200	4	0	20	1	0	0	0	0	0	0	0	0	0	0	0	0	0	0	0	0
51	15	[11	19	66		4	90	17	1025	97.	30	33.63	0	20	0	0	20	1	0	1	1	0	0	0	0	0	0	0	0	0	0	0	0	0

(*continued on next page*)

Table A (*continued*)

	4	1]					5		5																						
51	155		19	67		5	90	175	1025	97.5	30	33.63	1	160	12	0	20	1	0	1	1	0	0	0	0	0	0	0	0	0	0
51	156		19	68		4	0	175	1025	97.5	30	33.63	0	20	0	0	20	1	0	1	1	0	0	0	0	0	0	0	0	0	0	0
52	157		20	69		10	90	370	1300	80	30	177.58	1	160	10	0	20	1	0	1	0	0	0	0	0	0	0	0	0	0	0	0
52	158		20	70		8	90	370	1300	80	30	177.58	1	160	10	0	20	1	0	0	0	0	0	0	0	0	0	0	0	0	0	0
52	159		20	71		8	45	370	1300	80	30	177.58	1	160	10	0	20	1	0	1	0	0	0	0	0	0	0	0	0	0	0	0
52	160		20	72		7	45	370	1300	80	30	177.58	1	160	10	0	20	1	0	0	0	0	0	0	0	0	0	0	0	0	0	0
52	161	[112]	20	73		14	0	370	1300	80	30	177.58	1	160	10	0	20	1	0	1	0	0	0	0	0	0	0	0	0	0	0	0
52	162		20	74		10	0	370	1300	80	30	177.58	1	160	10	0	20	1	0	0	0	0	0	0	0	0	0	0	0	0	0	0
52	163		20	75		3	90	370	1300	80	30	177.58	1	300	2	0	20	1	0	1	0	0	0	0	0	0	0	0	0	0	0	0
52	164		20	76		5	90	370	1300	80	30	177.58	1	300	2	0	20	1	0	0	0	0	0	0	0	0	0	0	0	0	0	0
52	165		20	77		10	0	370	1300	80	30	177.58	1	300	2	0	20	1	0	1	0	0	0	0	0	0	0	0	0	0	0	0
52	166		20	78		4	0	370	1300	80	30	177.58	1	300	2	0	20	1	0	0	0	0	0	0	0	0	0	0	0	0	0	0
53	167		21	79		11	90	350	1650	130	50	392.70	1	200	4	0	20	1	0	1	1	0	0	0	0	0	0	0	0	0	0	0
53	168	[113]	21	80		28	90	350	1650	130	50	392.70	1	200	4	0	20	1	0	0	0	0	0	0	0	0	0	0	0	0	0	0
53	169		21	81		17	90	350	1650	130	50	392.70	1	200	4	0	20	1	0	0	0	0	1	0	0	0	0	0	0	0	0	0
54	170	[114]	22	82		18	90	380	1350	145	50	883.57	1	300	2	0	20	1	0	1	1	0	0	0	0	0	0	0	0	0	0	0
55	171		1	0		7	90	1030	425	130	30	28.90	0	20	0	0	20	1	0	0	0	0	0	0	0	0	0	0	0	0	0	0
55	172	[55]	1	1		14	90	1030	425	130	30	28.90	0	20	0	0	20	1	0	1	0	0	0	0	0	0	0	0	0	0	0	0
55	173		1	2		16	90	1030	425	130	30	28.90	0	20	0	0	20	1	0	1	1	0	0	0	0	0	0	0	0	0	0	0
56	174		2	3		10	0	350	1000	100	30	173.18	0	20	0	0	20	1	0	1	1	0	0	0	0	0	0	0	0	0	0	0
56	175		2	4		10	90	350	1000	100	30	173.18	0	20	0	0	20	1	0	1	1	0	0	0	0	0	0	0	0	0	0	0
56	176	[115]	2	5		10	45	350	1000	100	30	173.18	0	20	0	0	20	1	0	1	1	0	0	0	0	0	0	0	0	0	0	0
56	177		2	6		10	90	350	1000	100	30	173.18	0	20	0	0	20	1	0	0	0	0	0	0	0	0	0	0	0	0	0	0
56	178		2	7		10	45	350	1000	100	30	173.18	0	20	0	0	20	1	0	0	0	0	0	0	0	0	0	0	0	0	0	0
57	179	[116]	3	8	SS316	6	0	250	800	100	50	81.29	0	20	0	0	20	1	0	1	1	0	0	0	0	0	0	0	1	0	0	0
57	180		3	9		6	0	250	800	100	50	81.29	0	20	0	0	20	1	0	1	1	0	0	0	0	0	0	0	1	0	0	0
58	181		4	10		18	90	190	750	120	30	603.30	0	20	0	0	20	1	0	0	1	0	0	0	0	0	0	0	0	0	0	0
58	182	[117]	4	11		11	90	190	750	120	30	603.30	0	20	0	0	20	1	0	1	1	0	0	0	0	0	0	0	0	0	0	0
58	183		4	12		10	90	190	750	120	30	603.30	1	900	2	0	20	1	0	0	1	0	0	0	0	0	0	0	0	0	0	0
58	184		4	13		13	90	190	750	120	30	603.30	1	900	2	0	20	1	0	1	1	0	0	0	0	0	0	0	0	0	0	0
59	185	[118]	5	14		19	90	90	1000	150	30	86.39	1	500	1	0	20	1	0	0	1	0	0	0	0	0	0	0	0	0	0	0
60	186	[119]	6	15		6	0	175	750	100	30	27.00	0	20	0	0	20	1	0	0	0	1	0	0	0	0	0	0	0	0	0	0
60	18		6	16		6	0	17	550	10	50	27.00	0	20	0	0	20	1	0	0	0	1	0	0	0	0	0	0	0	0	0	0

(*continued on next page*)

Table A (*continued*)

	7						5		0																						
60	188		6	17	7	45	175	750	1000	30	27.00	0	20	0	0	20	1	0	0	0	1	0	0	0	0	0	0	0	0	0	0
60	189		6	18	8	45	175	550	1000	50	27.00	0	20	0	0	20	1	0	0	0	1	0	0	0	0	0	0	0	0	0	0
60	190		6	19	10	90	175	750	1000	30	27.00	0	20	0	0	20	1	0	0	0	1	0	0	0	0	0	0	0	0	0	0
60	191		6	20	8	90	175	550	1000	50	27.00	0	20	0	0	20	1	0	0	0	1	0	0	0	0	0	0	0	0	0	0
61	192		7	21	7	90	2000	1000	110	50	661.87	1	1038	1	0	20	1	0	0	0	0	0	0	0	0	0	0	0	0	0	0
61	193		7	22	8	90	2000	1000	110	50	172.45	1	1038	1	0	20	1	0	0	0	0	0	0	0	0	0	0	0	0	0	0
61	194		7	23	8	90	195	1083	90	20	661.87	1	1038	1	0	20	1	0	0	0	0	0	0	0	0	0	0	0	0	0	0
61	195	[120]	7	24	8	90	195	1083	90	20	172.45	1	1038	1	0	20	1	0	0	0	0	0	0	0	0	0	0	0	0	0	0
61	196		7	25	8	90	2000	1000	110	50	661.87	1	1038	1	0	20	1	0	1	1	0	0	0	0	0	0	0	0	0	0	0
61	197		7	26	7	90	2000	1000	110	50	172.45	1	1038	1	0	20	1	0	1	1	0	0	0	0	0	0	0	0	0	0	0
61	198		7	27	5	90	195	1083	90	20	172.45	1	1038	1	0	20	1	0	1	1	0	0	0	0	0	0	0	0	0	0	0
62	199	[121]	8	28	4	0	195	1083	90	20	272.93	0	20	0	0	20	1	0	1	1	0	0	0	0	0	0	0	0	0	0	0
63	200		9	29	12	90	275	700	1000	50	1005.31	1	620	1.5	0	20	1	0	0	0	0	0	0	0	0	0	0	0	0	0	0
63	201	[122]	9	30	12	90	275	700	1000	50	1005.31	1	620	1.5	0	20	1	0	0	1	0	0	0	0	0	0	0	0	0	0	0
63	202		9	31	15	90	275	700	1000	50	60.00	1	620	1.5	0	20	1	0	0	0	0	0	0	0	0	0	0	0	0	0	0
63	203		9	32	15	90	275	700	1000	50	60.00	1	620	1.5	0	20	1	0	0	1	0	0	0	0	0	0	0	0	0	0	0
63	204		9	33	11	90	275	700	1000	50	60.00	1	620	1.5	0	20	1	0	0	1	0	0	0	0	0	0	0	0	0	0	0
64	205	[123]	10	34	22	90	245	960	1000	30	346.84	0	20	0	1	900	1000	2	0	1	0	0	0	0	0	0	0	0	0	0	0
64	206		10	35	21	90	245	960	1000	30	346.84	0	20	0	0	20	1	0	0	1	0	0	0	0	0	0	0	0	0	0	0
65	207		11	36	7	0	250	1083	90	20	45.89	0	20	0	0	20	1	0	0	0	0	0	0	0	0	0	0	0	0	0	0
65	208		11	37	8	90	250	1083	90	20	45.89	0	20	0	0	20	1	0	0	0	0	0	0	0	0	0	0	0	0	0	0
65	209	[124]	11	38	5	0	250	1083	90	40	45.89	0	20	0	0	20	1	0	0	0	0	0	0	0	0	0	0	0	0	0	0
65	210		11	39	6	90	250	1083	90	40	45.89	0	20	0	0	20	1	0	0	0	0	0	0	0	0	0	0	0	0	0	0
66	211	[125]	12	40	16	0	195	1083	90	20	144.00	0	20	0	0	20	1	0	0	0	0	0	0	0	0	0	0	0	0	0	1
66	212		12	41	14	0	195	1083	90	20	144.00	0	20	0	0	20	1	0	0	0	0	0	0	0	0	0	0	0	0	0	1
67	213		13	42	4	90	195	1083	90	20	294.52	0	20	0	0	20	1	0	1	1	0	0	0	0	0	0	0	0	0	0	0
67	214	[126]	13	43	4	90	195	1083	90	20	294.52	1	900	0.167	0	20	1	0	1	1	0	0	0	0	0	0	0	0	0	0	0
67	215		13	44	5	90	195	1083	90	20	294.52	1	1050	0.167	0	20	1	0	1	1	0	0	0	0	0	0	0	0	0	0	0
68	216	[127]	14	45	10	0	180	1200	60	30	161.01	1	650	2	0	20	1	0	1	0	0	0	0	0	0	0	0	0	0	0	0
69	217	[23]	15	46	15	90	320	2400	100	50	190.85	0	20	0	0	20	1	0	0	0	0	0	0	0	0	0	0	0	0	0	0

(*continued on next page*)

Table A (*continued*)

70	218	[128]	16	47		10	90	275	760	120	50	171.26	0	20	0	0	20	1	0	0	0	0	0	0	0	0	0	0	0	0	0
70	219		16	48		14	90	275	760	120	50	171.26	0	20	0	0	20	1	0	0	0	0	0	0	0	1	0	0	0	0	0
70	220		16	49		13	90	275	760	120	50	171.26	0	20	0	0	20	1	0	1	0	0	0	0	0	0	0	0	0	0	0
71	221	[129]	17	50		9	90	113	600	80	20	933.05	0	20	0	0	20	1	0	1	0	0	0	0	0	0	0	0	0	0	0

Appendix B:. Additional results of probabilistic fatigue curves

The Appendix reports additional results for other external validation datasets for all three alloys, four per material. Of course, to save experimental costs in fatigue testing, it is preferable to adopt as less training points as possible. Hence, for conciseness, this additional evaluation has been reported only at 50 training points. Fig. B1 reports the Ti6Al4V external datasets 16 (a), 21 (b), 37 (c) and 85 (d). Fig. B2 shows the AlSi10Mg external datasets 45 (a), 54 (b), 57 (c) and 81 (d). Finally Fig. B3 reports the SS316L external datasets 1 (a), 2 (b), 35 (c) and 40 (d). The results show that the TL procedures can output a usable design R90C90 PSN curve for all cases, proving the trustworthiness of the TL framework.

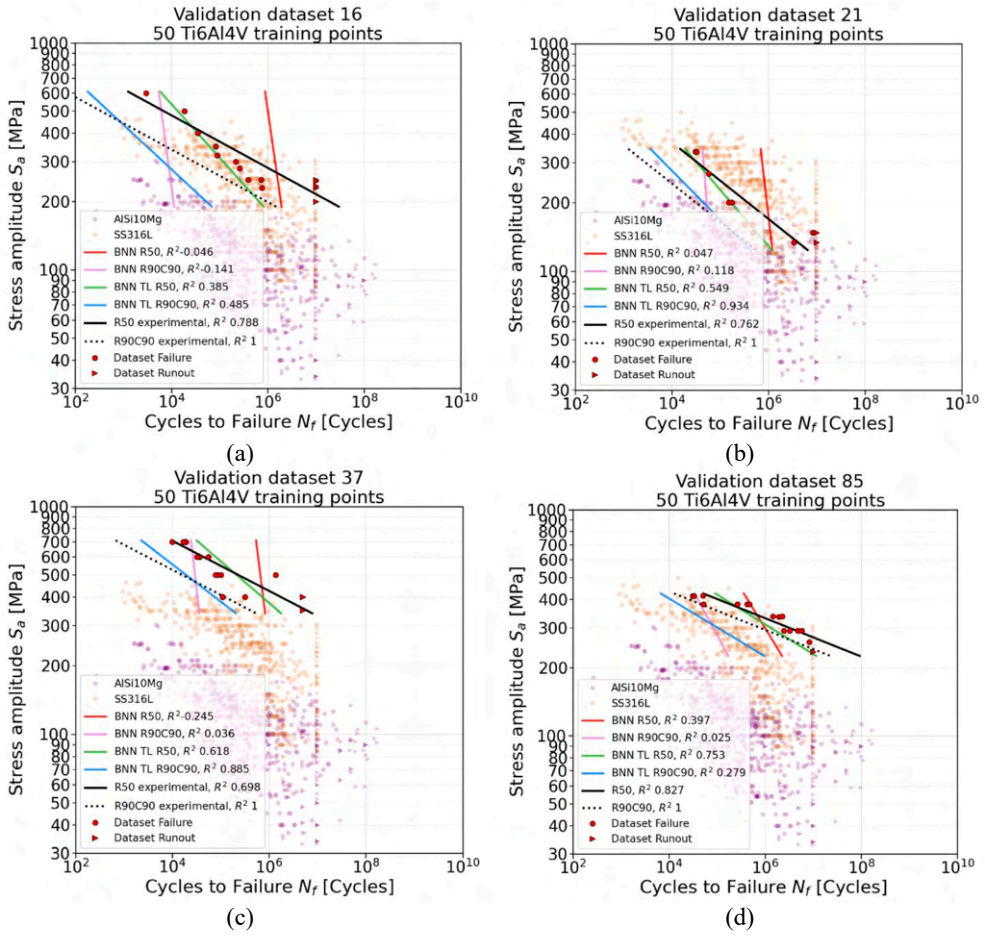


Fig. B1. Additional PSN curves to assess the effectiveness of TL on Ti6Al4V from a BNN pretrained on AlSi10Mg (purple points) and SS316L (orange points) at 50 training points for the external datasets 16 (a), 21 (b), 37 (c) and 85 (d). The experimental datasets (red points and triangles) have been validated to output the R50 (red without TL and green with TL) and R90C90 life (magenta without TL and blue with TL) with and without TL. In solid black the experimental R50 line, while in dashed black the experimental R90C90 line.

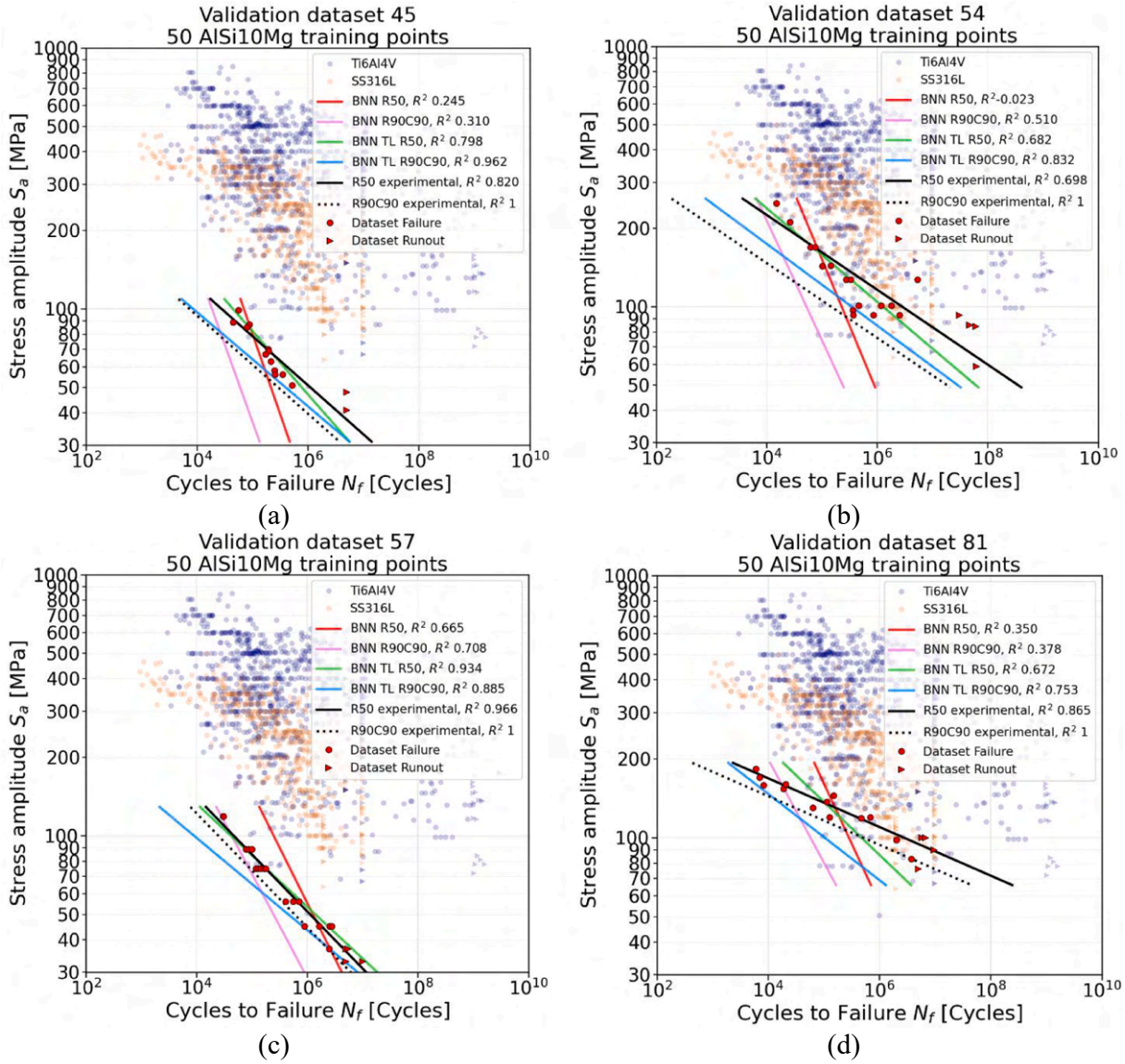


Fig. B2. Additional PSN curves to assess the effectiveness of TL on AlSi10Mg from a BNN pretrained on Ti6Al4V (blue points) and SS316L (orange points) at 50 training points for the external datasets 45 (a), 54 (b), 57 (c) and 81 (d). The experimental datasets (red points and triangles) have been validated to output the R50 (red without TL and green with TL) and R90C90 life (magenta without TL and blue with TL) with and without TL. In solid black the experimental R50 line, while in dashed black the experimental R90C90 line.

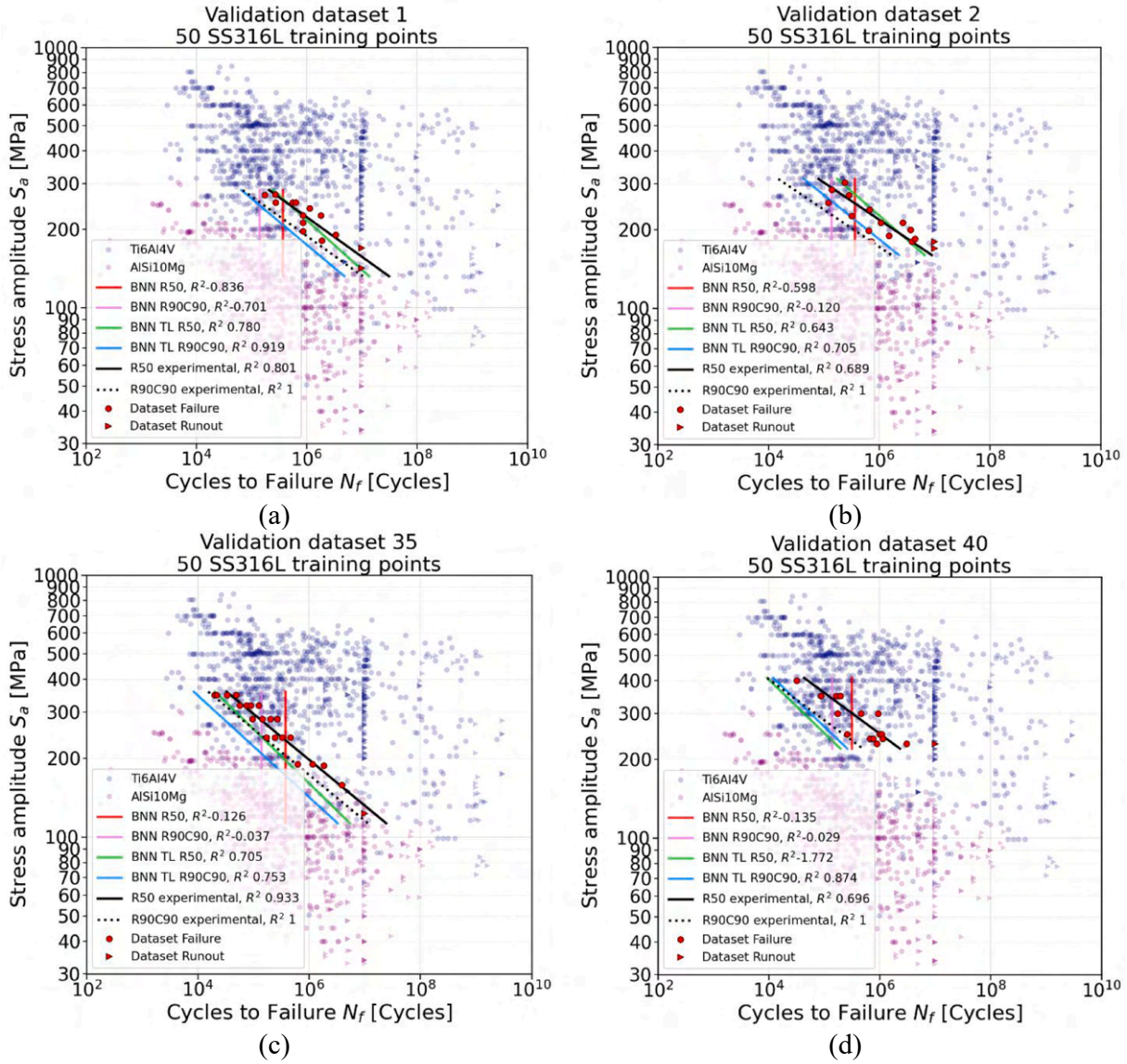


Fig. B3. Additional PSN curves to assess the effectiveness of TL on SS316L from a BNN pretrained on Ti6Al4V (blue points) and AlSi10Mg (purple points) at 50 training points for the external datasets 1 (a), 2 (b), 35 (c) and 40 (d). The experimental datasets (red points and triangles) have been validated to output the R50 (red without TL and green with TL) and R90C90 life (magenta without TL and blue with TL) with and without TL. In solid black the experimental R50 line, while in dashed black the experimental R90C90 line.

Appendix C. Supplementary data

Supplementary data to this article can be found online at https://doi.org/10.1016/j.engfailanal.2026.111075.

Data availability

Data will be made available on request.

References

[1] J. Plocher, A. Panesar, Review on design and structural optimisation in additive manufacturing: Towards next-generation lightweight structures, Mater. Des. 183 (2019), https://doi.org/10.1016/j.matdes.2019.108164.

[2] R. Caivano, A. Tridello, M. Codegone, G. Chiandussi, A new methodology for thermostructural topology optimization: Analytical definition and validation, Proceedings of the Institution of Mechanical Engineers, Part L: Journal of Materials: Design and Applications 235 (2021). 10.1177/1464420720970246.
[3] C. Boursier Niutta, A. Tridello, G. Barletta, N. Gallo, A. Baroni, F. Berto, D.S. Paolino, Defect-Driven topology optimization for fatigue design of additive manufacturing structures: Application on a real industrial aerospace component, Eng. Fail. Anal. 142 (2022), https://doi.org/10.1016/j.engfailanal.2022.106737.
[4] M. Benedetti, A. du Plessis, R.O. Ritchie, M. Dallago, N. Razavi, F. Berto, Architected cellular materials: a review on their mechanical properties towards fatigue-tolerant design and fabrication, Materials Science and Engineering r: Reports 144 (2021), https://doi.org/10.1016/j.mser.2021.100606.
[5] W. Wu, W. Hu, G. Qian, H. Liao, X. Xu, F. Berto, Mechanical design and multifunctional applications of chiral mechanical metamaterials: a review, Mater. Des. 180 (2019), https://doi.org/10.1016/j.matdes.2019.107950.
[6] C.B. Niutta, R. Ciardiello, A. Tridello, Experimental and Numerical Investigation of a Lattice Structure for Energy Absorption: Application to the Design of an Automotive Crash Absorber, Polymers (Basel). 14 (2022), https://doi.org/10.3390/polym14061116.
[7] I. Gibson, D.W. Rosen, B. Stucker, Additive Manufacturing Technologies: Rapid Prototyping to Direct Digital Manufacturing (2010), https://doi.org/10.1007/978-1-4419-1120-9.
[8] M. Yakout, M.A. Elbestawi, S.C. Veldhuis, A review of metal additive manufacturing technologies, Solid State Phenom. (2018), https://doi.org/10.4028/www.scientific.net/SSP.278.1.
[9] W.E. Frazier, Metal additive manufacturing: a review, J. Mater. Eng. Perform. 23 (2014), https://doi.org/10.1007/s11665-014-0958-z.
[10] A. Centola, A. Ciampaglia, C. Boursier Niutta, F. Berto, D.S. Paolino, A. Tridello, Data driven topology optimization of AM parts accounting for process-affected fatigue performance: Application to automotive and aerospace components, Int. J. Fatigue (2026) 109481, https://doi.org/10.1016/J.IJFATIGUE.2026.109481.
[11] Y. Yamashita, T. Murakami, R. Mihara, M. Okada, Y. Murakami, Defect Analysis and Fatigue Design Basis for Ni-based Superalloy 718 manufactured by Additive Manufacturing, Procedia Struct. Integrity (2017), https://doi.org/10.1016/j.prostr.2017.11.054.
[12] A. Yadollahi, N. Shamsaei, Additive manufacturing of fatigue resistant materials: challenges and opportunities, Int. J. Fatigue 98 (2017), https://doi.org/10.1016/j.ijfatigue.2017.01.001.
[13] Y. Murakami, H. Masuo, Y. Tanaka, M. Nakatani, Defect Analysis for Additively Manufactured Materials in Fatigue from the viewpoint of Quality Control and Statistics of Extremes, Procedia Struct. Integrity 19 (2019) 113–122, https://doi.org/10.1016/J.PROSTR.2019.12.014.
[14] N. Sanaei, A. Fatemi, Defects in additive manufactured metals and their effect on fatigue performance: a state-of-the-art review, Prog. Mater Sci. 117 (2021) 100724, https://doi.org/10.1016/J.PMATSCI.2020.100724.
[15] C. Ronchei, S. Vantadori, A. Carpinteri, Fatigue lifetime assessment of AM metallic components according to a strain-based criterion, Int. J. Fatigue 156 (2022) 106674, https://doi.org/10.1016/J.IJFATIGUE.2021.106674.
[16] S. Leuders, T. Lieneke, S. Lammers, T. Tröster, T. Niendorf, On the fatigue properties of metals manufactured by selective laser melting - the role of ductility, J. Mater. Res. 29 (2014), https://doi.org/10.1557/jmr.2014.157.
[17] L. Du, G. Qian, L. Zheng, Y. Hong, Influence of processing parameters of selective laser melting on high-cycle and very-high-cycle fatigue behaviour of Ti-6Al-4V, Fatigue Fract. Eng. Mater. Struct. 44 (2021), https://doi.org/10.1111/ffe.13361.
[18] A. Tridello, J. Fiocchi, C.A. Biffi, G. Chiandussi, M. Rossetto, A. Tuissi, D.S. Paolino, VHCF response of Gaussian SLM AlSi10Mg specimens: effect of a stress relief heat treatment, Int. J. Fatigue 124 (2019), https://doi.org/10.1016/j.ijfatigue.2019.02.020.
[19] A. Tridello, J. Fiocchi, C.A. Biffi, M. Rossetto, A. Tuissi, D.S. Paolino, Size-effects affecting the fatigue response up to 109 cycles (VHCF) of SLM AlSi10Mg specimens produced in horizontal and vertical directions, Int. J. Fatigue 160 (2022), https://doi.org/10.1016/j.ijfatigue.2022.106825.
[20] F. Calignano, D. Manfredi, E.P. Ambrosio, L. Iuliano, P. Fino, Influence of process parameters on surface roughness of aluminum parts produced by DMLS, Int. J. Adv. Manuf. Technol. 67 (2013), https://doi.org/10.1007/s00170-012-4688-9.
[21] S. Beretta, S. Romano, A comparison of fatigue strength sensitivity to defects for materials manufactured by AM or traditional processes, Int. J. Fatigue 94 (2017), https://doi.org/10.1016/j.ijfatigue.2016.06.020.
[22] H. Masuo, Y. Tanaka, S. Morokoshi, H. Yagura, T. Uchida, Y. Yamamoto, Y. Murakami, Influence of defects, surface roughness and HIP on the fatigue strength of Ti-6Al-4V manufactured by additive manufacturing, Int. J. Fatigue 117 (2018), https://doi.org/10.1016/j.ijfatigue.2018.07.020.
[23] K. Solberg, S. Guan, N. Razavi, T. Welo, K.C. Chan, F. Berto, Fatigue of additively manufactured 316L stainless steel: the influence of porosity and surface roughness, Fatigue Fract. Eng. Mater. Struct. 42 (2019), https://doi.org/10.1111/ffe.13077.
[24] J. Chen, Y. Liu, Fatigue property prediction of additively manufactured Ti-6Al-4V using probabilistic physics-guided learning, Addit. Manuf. 39 (2021) 101876, https://doi.org/10.1016/J.ADDMA.2021.101876.
[25] J. Horňas, J. Běhal, P. Homola, S. Senck, M. Holzleitner, N. Godja, Z. Pásztor, B. Hegedüs, R. Doubrava, R. Růžek, L. Petrusová, Modelling fatigue life prediction of additively manufactured Ti-6Al-4V samples using machine learning approach, Int. J. Fatigue 169 (2023) 107483, https://doi.org/10.1016/J.IJFATIGUE.2022.107483.
[26] E. Salvati, A. Tognan, L. Laurenti, M. Pelegatti, F. De Bona, A defect-based physics-informed machine learning framework for fatigue finite life prediction in additive manufacturing, Mater. Des. 222 (2022) 111089, https://doi.org/10.1016/J.MATDES.2022.111089.
[27] A. Cutolo, N. Lammens, K. Vanden Boer, H. Erdelyi, M. Schulz, G.K. Muralidharan, L. Thijs, C. Elangeswaran, B. Van Hooreweder, Fatigue life prediction of a L-PBF component in Ti-6Al-4V using sample data, FE-based simulations and machine learning, Int. J. Fatigue 167 (2023) 107276. 10.1016/J.IJFATIGUE.2022.107276.
[28] H. Wang, B. Li, F.Z. Xuan, Fatigue-life prediction of additively manufactured metals by continuous damage mechanics (CDM)-informed machine learning with sensitive features, Int. J. Fatigue 164 (2022) 107147, https://doi.org/10.1016/J.IJFATIGUE.2022.107147.
[29] X. Wang, M. Braun, Explainable machine learning-based fatigue assessment of 316L stainless steel fabricated by laser-powder bed fusion, Int. J. Fatigue 190 (2025), https://doi.org/10.1016/j.ijfatigue.2024.108588.
[30] J. Du, X. Yang, T. Zhu, T. Lu, N. Yao, Y. Chen, K. Li, X. Chen, G. Ma, B. Sun, X.C. Zhang, S.T. Tu, A universal high-cycle fatigue life prediction of additive manufacturing medium-entropy alloys via machine learning and nondestructive tests, Int. J. Fatigue 204 (2026), https://doi.org/10.1016/j.ijfatigue.2025.109360.
[31] S. Yang, Z. Zhang, R. Guo, Z. Zhan, Physics-informed machine learning for high-cycle fatigue of AM Ti6Al4V: Life prediction and correlation analysis, Int. J. Fatigue 203 (2026), https://doi.org/10.1016/j.ijfatigue.2025.109296.
[32] A. Centola, A. Tridello, A. Ciampaglia, F. Berto, D.S. Paolino, Review on machine learning techniques for the assessment of the fatigue response of additively manufactured metal parts, Fatigue Fract. Eng. Mater. Struct. (2024), https://doi.org/10.1111/ffe.14326.
[33] A. Centola, A. Ciampaglia, A. Tridello, D.S. Paolino, Machine learning methods to predict the fatigue life of selectively laser melted Ti6Al4V components, Fatigue Fract. Eng. Mater. Struct. 46 (2023), https://doi.org/10.1111/ffe.14125.
[34] A. Tridello, A. Ciampaglia, F. Berto, D.S. Paolino, Assessment of the critical defect in Additive Manufacturing Components through Machine Learning Algorithms, Applied Sciences (switzerland) 13 (2023), https://doi.org/10.3390/app13074294.
[35] E. Maleki, S. Bagherifard, M. Guagliano, Correlation of residual stress, hardness and surface roughness with crack initiation and fatigue strength of surface treated additive manufactured AlSi10Mg: Experimental and machine learning approaches, J. Mater. Res. Technol. 24 (2023) 3265–3283, https://doi.org/10.1016/J.JMRT.2023.03.193.
[36] L. Dang, X. He, D. Tang, Y. Li, T. Wang, A fatigue life prediction approach for laser-directed energy deposition titanium alloys by using support vector regression based on pore-induced failures, Int. J. Fatigue 159 (2022), https://doi.org/10.1016/j.ijfatigue.2022.106748.
[37] M. Zhang, C.N. Sun, X. Zhang, P.C. Goh, J. Wei, D. Hardacre, H. Li, High cycle fatigue life prediction of laser additive manufactured stainless steel: a machine learning approach, Int. J. Fatigue 128 (2019) 105194, https://doi.org/10.1016/J.IJFATIGUE.2019.105194.
[38] M. Raissi, P. Perdikaris, G.E. Karniadakis, Physics-informed neural networks: a deep learning framework for solving forward and inverse problems involving nonlinear partial differential equations, J. Comput. Phys. 378 (2019) 686–707, https://doi.org/10.1016/J.JCP.2018.10.045.

[39] A. Ciampaglia, A. Tridello, D.S. Paolino, F. Berto, Data driven method for predicting the effect of process parameters on the fatigue response of additive manufactured AlSi10Mg parts, Int. J. Fatigue 170 (2023) 107500, https://doi.org/10.1016/J.IJFATIGUE.2023.107500.
[40] A. Ciampaglia, A. Tridello, F. Berto, D. Paolino, Data-driven method to assess the influence of process parameters on the fatigue response of additively manufactured Ti6Al4V, Procedia Struct. Integrity 47 (2023) 56–69, https://doi.org/10.1016/j.prostr.2023.06.041.
[41] Y. Murakami, Metal Fatigue: Effects of Small Defects and Nonmetallic Inclusions (2019), https://doi.org/10.1016/C2016-0-05272-5.
[42] A. Centola, A. Ciampaglia, D.S. Paolino, A. Tridello, Probabilistic Machine Learning for preventing fatigue failures in Additively Manufactured SS316L, Eng. Fail. Anal. 168 (2025) 109081, https://doi.org/10.1016/J.ENGFAILANAL.2024.109081.
[43] Y.L. Lee, J. Pan, R. Hathaway, M. Barkey, Fatigue Testing and Analysis (2005), https://doi.org/10.1016/B978-0-7506-7719-6.X5000-3.
[44] C. Blundell, J. Cornebise, K. Kavukcuoglu, D. Wierstra, Weight uncertainty in neural networks. In: 32nd International Conference on Machine Learning, 2015, 2015..
[45] V.H. Mochi, H.H.L. Núñez, K.S.B. Ribeiro, G.S. Venter, Real-time prediction of deposited bead width in L-DED using semi-supervised transfer learning, Int. J. Adv. Manuf. Technol. 129 (2023), https://doi.org/10.1007/s00170-023-12658-6.
[46] O.H. Anidjar, R. Lang, M. Mega, Transfer Learning Methods for Fractographic Detection of Fatigue Crack Initiation in Additive Manufacturing, IEEE Access 12 (2024), https://doi.org/10.1109/ACCESS.2024.3350709.
[47] S. Goswami, C. Anitescu, S. Chakraborty, T. Rabczuk, Transfer learning enhanced physics informed neural network for phase-field modeling of fracture, Theor. Appl. Fract. Mech. 106 (2020), https://doi.org/10.1016/j.tafmec.2019.102447.
[48] H. Wu, Z.M. Fan, L. Gan, Feature transfer Learning for Fatigue Life Prediction of Additive Manufactured Metals with Small Samples, Fatigue Fract. Eng. Mater. Struct. 48 (2025) 467–486, https://doi.org/10.1111/ffe.14497.
[49] Q. Zhai, Z. Liu, P. Zhu, A transfer learning enhanced physics-informed neural network for predicting fatigue life of megacasting alloy with limited data sizes, Int. J. Fatigue 200 (2025), https://doi.org/10.1016/j.ijfatigue.2025.109129.
[50] D.S. Paolino, G. Chiandussi, M. Rossetto, A unified statistical model for S-N fatigue curves: Probabilistic definition, Fatigue Fract. Eng. Mater. Struct. 36 (2013), https://doi.org/10.1111/j.1460-2695.2012.01711.x.
[51] G.E. Hinton, D. van Camp, Keeping neural networks simple by minimizing the description length of the weights, In (1993), https://doi.org/10.1145/168304.168306.
[52] X. Ying, An Overview of Overfitting and its Solutions, J. Phys. Conf. Ser. (2019), https://doi.org/10.1088/1742-6596/1168/2/022022.
[53] A. Soltani-Tehrani, M. Habibnejad-Korayem, S. Shao, M. Haghshenas, N. Shamsaei, Ti-6Al-4V powder characteristics in laser powder bed fusion: the effect on tensile and fatigue behavior, Addit. Manuf. 51 (2022) 102584, https://doi.org/10.1016/J.ADDMA.2021.102584.
[54] A. Tridello, J. Fiocchi, C.A. Biffi, G. Chiandussi, M. Rossetto, A. Tuissi, D.S. Paolino, Effect of microstructure, residual stresses and building orientation on the fatigue response up to 109 cycles of an SLM AlSi10Mg alloy, Int. J. Fatigue 137 (2020) 105659, https://doi.org/10.1016/J.IJFATIGUE.2020.105659.
[55] A.B. Spierings, T.L. Starr, K. Wegener, Fatigue performance of additive manufactured metallic parts, Rapid Prototyp. J. 19 (2013), https://doi.org/10.1108/13552541311302932.
[56] B. Blinn, M. Klein, C. Gläßner, M. Smaga, J.C. Aurich, T. Beck, An investigation of the microstructure and fatigue behavior of additively manufactured AISI 316L stainless steel with regard to the influence of heat treatment, Metals (basel). 8 (2018), https://doi.org/10.3390/met8040220.
[57] P.M. Cerezo, J.A. Aguilera, A. Garcia-Gonzalez, P. Lopez-Crespo, Influence of Porosity on Fatigue Behaviour of 18Ni300 Steel SLM CT Specimens at Various Angles, Materials 17 (2024), https://doi.org/10.3390/ma17020432.
[58] M. Bakhtiarian, H. Omidvar, A. Mashhuriazar, Z. Sajuri, C.H. Gur, The effects of SLM process parameters on the relative density and hardness of austenitic stainless steel 316L, J. Mater. Res. Technol. 29 (2024), https://doi.org/10.1016/j.jmrt.2024.01.237.
[59] G. Kasperovich, J. Hausmann, Improvement of fatigue resistance and ductility of TiAl6V4 processed by selective laser melting, J. Mater. Process. Technol. 220 (2015), https://doi.org/10.1016/j.jmatprotec.2015.01.025.
[60] N. Sanaei, A. Fatemi, Defects in additive manufactured metals and their effect on fatigue performance: a state-of-the-art review, Prog. Mater Sci. 117 (2021), https://doi.org/10.1016/j.pmatsci.2020.100724.
[61] M. Mohseni, M.S. Sadeghi, A. Hemasian Etefagh, S.M. Nikouei, M. Khajehzadeh, The effect of selective laser melting process parameters and remelting scanning strategy on relative density and surface hardness of stainless steel 316L, Proceedings of the Institution of Mechanical Engineers, Part e: Journal of Process Mechanical Engineering (2023), https://doi.org/10.1177/09544089231207809.
[62] G. Kasperovich, J. Haubrich, J. Gussone, G. Requena, Correlation between porosity and processing parameters in TiAl6V4 produced by selective laser melting, Mater. Des. 105 (2016), https://doi.org/10.1016/j.matdes.2016.05.070.
[63] J. Günther, D. Krewerth, T. Lippmann, S. Leuders, T. Tröster, A. Weidner, H. Biermann, T. Niendorf, Fatigue life of additively manufactured Ti–6Al–4V in the very high cycle fatigue regime, Int. J. Fatigue 94 (2017), https://doi.org/10.1016/j.ijfatigue.2016.05.018.
[64] Y.N. Hu, S.C. Wu, P.J. Withers, J. Zhang, H.Y.X. Bao, Y.N. Fu, G.Z. Kang, The effect of manufacturing defects on the fatigue life of selective laser melted Ti-6Al-4V structures, Mater. Des. 192 (2020) 108708, https://doi.org/10.1016/J.MATDES.2020.108708.
[65] X. Zhao, S. Li, M. Zhang, Y. Liu, T.B. Sercombe, S. Wang, Y. Hao, R. Yang, L.E. Murr, Comparison of the microstructures and mechanical properties of Ti–6Al–4V fabricated by selective laser melting and electron beam melting, Mater. Des. 95 (2016) 21–31, https://doi.org/10.1016/J.MATDES.2015.12.135.
[66] M. Fousová, D. Vojtěch, K. Doubrava, M. Daniel, C.F. Lin, Influence of inherent surface and internal defects on mechanical properties of additively manufactured Ti6Al4V alloy: Comparison between selective laser melting and electron beam melting, Materials 11 (2018), https://doi.org/10.3390/ma11040537.
[67] Q. Jiang, S. Li, C. Zhou, B. Zhang, Y. Zhang, Effects of laser shock peening on the ultra-high cycle fatigue performance of additively manufactured Ti6Al4V alloy, Opt. Laser Technol. 144 (2021) 107391, https://doi.org/10.1016/J.OPTLASTEC.2021.107391.
[68] C. Sun, W. Chi, W. Wang, Y. Duan, Characteristic and mechanism of crack initiation and early growth of an additively manufactured Ti-6Al-4V in very high cycle fatigue regime, Int. J. Mech. Sci. 205 (2021) 106591, https://doi.org/10.1016/J.IJMECSCI.2021.106591.
[69] W. Eric, E. Claus, S. Shafaqat, W. Frank, High cycle fatigue (HCF) performance of Ti-6Al-4V alloy processed by selective laser melting, Adv. Mat. Res. (2013), https://doi.org/10.4028/www.scientific.net/AMR.816-817.134.
[70] H. Gong, K. Rafi, H. Gu, G.D. Janaki Ram, T. Starr, B. Stucker, Influence of defects on mechanical properties of Ti–6Al–4 V components produced by selective laser melting and electron beam melting, Mater. Des. 86 (2015) 545–554, https://doi.org/10.1016/J.MATDES.2015.07.147.
[71] J.M. Alegre, A. Díaz, R. García, L.B. Peral, I.I. Cuesta, Effect of HIP post-processing at 850 °C/200 MPa in the fatigue behavior of Ti-6Al-4V alloy fabricated by Selective Laser Melting, Int. J. Fatigue 163 (2022) 107097, https://doi.org/10.1016/J.IJFATIGUE.2022.107097.
[72] N. Macallister, T.H. Becker, Fatigue life estimation of additively manufactured Ti-6Al-4V: Sensitivity, scatter and defect description in Damage-tolerant models, Acta Mater. 237 (2022) 118189, https://doi.org/10.1016/J.ACTAMAT.2022.118189.
[73] K. Mertova, J. Dzugan, M. Roudnicka, Fatigue properties of SLM-produced Ti6Al4V with various post-processing processes, IOP Conf. Ser.: Mater. Sci. Eng. (2018), https://doi.org/10.1088/1757-899X/461/1/012052.
[74] X. Yan, S. Yin, C. Chen, R. Jenkins, R. Lupoi, R. Bolot, W. Ma, M. Kuang, H. Liao, J. Lu, M. Liu, Fatigue strength improvement of selective laser melted ti6al4v using ultrasonic surface mechanical attrition, Mater. Res. Lett. 7 (2019), https://doi.org/10.1080/21663831.2019.1609110.
[75] P. Kumar, U. Ramamurty, High cycle fatigue in selective laser melted Ti-6Al-4V, Acta Mater. 194 (2020), https://doi.org/10.1016/j.actamat.2020.05.041.
[76] R. Xin, L. Lan, C. Bai, S. Gao, B. He, J. Wang, Fatigue properties of selective laser melted Ti-6Al-4V alloy subjected to laser shock processing, J. Mater. Sci. 57 (2022), https://doi.org/10.1007/s10853-022-07019-9.
[77] K. Dietrich, J. Diller, S. Dubiez-Le Goff, D. Bauer, P. Forêt, G. Witt, The influence of oxygen on the chemical composition and mechanical properties of Ti-6Al-4V during laser powder bed fusion (L-PBF), Addit. Manuf. 32 (2020) 100980, https://doi.org/10.1016/J.ADDMA.2019.100980.
[78] S. Lee, B. Rasoolian, D.F. Silva, J.W. Pegues, N. Shamsaei, Surface roughness parameter and modeling for fatigue behavior of additive manufactured parts: a non-destructive data-driven approach, Addit. Manuf. 46 (2021) 102094, https://doi.org/10.1016/J.ADDMA.2021.102094.

[79] M. Asherloo, Z. Wu, M. Heim, D. Nelson, M. Paliwal, A.D. Rollett, A. Mostafaei, Fatigue performance of laser powder bed fusion hydride-dehydride Ti-6Al-4V powder, Addit. Manuf. 59 (2022) 103117, https://doi.org/10.1016/J.ADDMA.2022.103117.

[80] L. Bhandari, V. Gaur, On study of process induced defects-based fatigue performance of additively manufactured Ti6Al4V alloy, Addit. Manuf. 60 (2022) 103227, https://doi.org/10.1016/J.ADDMA.2022.103227.

[81] B. Gillham, A. Yankin, F. McNamara, C. Tomonto, D. Taylor, R. Lupoi, Application of the Theory of critical Distances to predict the effect of induced and process inherent defects for SLM Ti-6Al-4V in high cycle fatigue, CIRP Ann. 70 (2021) 171–174, https://doi.org/10.1016/J.CIRP.2021.03.004.

[82] A. Ghiotti, R. Bertolini, M. Sorgato, A. Campagnolo, E. Savio, S. Bruschi, Ti6Al4V titanium alloy fatigue strength after AM- and machining-based process chains, CIRP Ann. 71 (2022) 461–464, https://doi.org/10.1016/J.CIRP.2022.04.021.

[83] A. Gupta, C.J. Bennett, W. Sun, High cycle fatigue performance evaluation of a laser powder bed fusion manufactured Ti-6Al-4V bracket for aero-engine applications, Eng. Fail. Anal. 140 (2022) 106494, https://doi.org/10.1016/J.ENGFAILANAL.2022.106494.

[84] K.F. Walker, Q. Liu, M. Brandt, Evaluation of fatigue crack propagation behaviour in Ti-6Al-4V manufactured by selective laser melting, Int. J. Fatigue 104 (2017) 302–308, https://doi.org/10.1016/J.IJFATIGUE.2017.07.014.

[85] H. Yu, F. Li, Z. Wang, X. Zeng, Fatigue performances of selective laser melted Ti-6Al-4V alloy: Influence of surface finishing, hot isostatic pressing and heat treatments, Int. J. Fatigue 120 (2019) 175–183, https://doi.org/10.1016/J.IJFATIGUE.2018.11.019.

[86] Z. Xu, A. Liu, X. Wang, B. Liu, M. Guo, Fatigue limit prediction model and fatigue crack growth mechanism for selective laser melting Ti6Al4V samples with inherent defects, Int. J. Fatigue 143 (2021) 106008, https://doi.org/10.1016/J.IJFATIGUE.2020.106008.

[87] R. Bertolini, A. Campagnolo, M. Sorgato, A. Ghiotti, S. Bruschi, G. Meneghetti, Fatigue strength of LPBF Ti6Al4V machined under flood and cryogenic lubri-cooling conditions, Int. J. Fatigue 162 (2022) 106973, https://doi.org/10.1016/J.IJFATIGUE.2022.106973.

[88] X. Yan, S. Yin, C. Chen, C. Huang, R. Bolot, R. Lupoi, M. Kuang, W. Ma, C. Coddet, H. Liao, M. Liu, Effect of heat treatment on the phase transformation and mechanical properties of Ti6Al4V fabricated by selective laser melting, J. Alloys Compd. 764 (2018) 1056–1071, https://doi.org/10.1016/J.JALLCOM.2018.06.076.

[89] K. Chang, E. Liang, W. Huang, X. Zhang, Y. Chen, J. Dong, R. Zhang, Microstructural feature and mechanical property in different building directions of additive manufactured Ti6Al4V alloy, Mater. Lett. 267 (2020) 127516, https://doi.org/10.1016/J.MATLET.2020.127516.

[90] P. Edwards, M. Ramulu, Fatigue performance evaluation of selective laser melted Ti–6Al–4V, Mater. Sci. Eng. A 598 (2014) 327–337, https://doi.org/10.1016/J.MSEA.2014.01.041.

[91] U. Segurajauregi, A. Álvarez-Vázquez, M. Muñiz-Calvente, Í. Urresti, H. Naveiras, Fatigue assessment of selective laser melted ti-6al-4v: Influence of speed manufacturing and porosity, Metals (basel). 11 (2021), https://doi.org/10.3390/met11071022.

[92] E.H. Jimenez, A. Kreitcberg, E. Moquin, V. Brailovski, Influence of Post-Processing Conditions on the Microstructure, Static, and Fatigue Resistance of Laser Powder Bed Fused Ti-6Al-4V Components, Journal of Manufacturing and Materials Processing 6 (2022), https://doi.org/10.3390/jmmp6040085.

[93] P. Ferro, A. Fabrizi, F. Berto, G. Savio, R. Meneghello, S. Rosso, Defects as a root cause of fatigue weakening of additively manufactured AlSi10Mg components, Theor. Appl. Fract. Mech. 108 (2020) 102611, https://doi.org/10.1016/J.TAFMEC.2020.102611.

[94] E. Brandl, U. Heckenberger, V. Holzinger, D. Buchbinder, Additive manufactured AlSi10Mg samples using Selective Laser Melting (SLM): Microstructure, high cycle fatigue, and fracture behavior, Mater. Des. 34 (2012) 159–169, https://doi.org/10.1016/J.MATDES.2011.07.067.

[95] M. Awd, S. Siddique, J. Johannsen, C. Emmelmann, F. Walther, Very high-cycle fatigue properties and microstructural damage mechanisms of selective laser melted AlSi10Mg alloy, Int. J. Fatigue 124 (2019), https://doi.org/10.1016/j.ijfatigue.2019.02.040.

[96] N.E. Uzan, R. Shneck, O. Yeheskel, N. Frage, Fatigue of AlSi10Mg specimens fabricated by additive manufacturing selective laser melting (AM-SLM), Mater. Sci. Eng. A 704 (2017) 229–237, https://doi.org/10.1016/J.MSEA.2017.08.027.

[97] N.E. Uzan, S. Ramati, R. Shneck, N. Frage, O. Yeheskel, On the effect of shot-peening on fatigue resistance of AlSi10Mg specimens fabricated by additive manufacturing using selective laser melting (AM-SLM), Addit. Manuf. 21 (2018) 458–464, https://doi.org/10.1016/J.ADDMA.2018.03.030.

[98] A. Ojha, W.J. Lai, Z. Li, C. Engler-Pinto, X. Su, Defect-based Fatigue Modeling for AlSi10Mg Produced by Laser Powder Bed Fusion Process, Minerals, Metals and Materials Series (2021), https://doi.org/10.1007/978-3-030-65261-6_7.

[99] J.G. Santos Macías, L. Zhao, D. Tingaud, B. Bacroix, G. Pyka, C. van der Rest, L. Ryelandt, A. Simar, Hot isostatic pressing of laser powder bed fusion AlSi10Mg: parameter identification and mechanical properties, J. Mater. Sci. 57 (2022), https://doi.org/10.1007/s10853-022-07027-9.

[100] W. Schneller, M. Leitner, S. Leuders, J.M. Sprauel, F. Grün, T. Pfeifer, O. Jantschner, Fatigue strength estimation methodology of additively manufactured metallic bulk material, Addit. Manuf. 39 (2021) 101688, https://doi.org/10.1016/J.ADDMA.2020.101688.

[101] C. Zhang, H. Zhu, H. Liao, Y. Cheng, Z. Hu, X. Zeng, Effect of heat treatments on fatigue property of selective laser melting AlSi10Mg, Int. J. Fatigue 116 (2018) 513–522, https://doi.org/10.1016/J.IJFATIGUE.2018.07.016.

[102] M. Muhammad, P.D. Nezhadfar, S. Thompson, A. Saharan, N. Phan, N. Shamsaei, A comparative investigation on the microstructure and mechanical properties of additively manufactured aluminum alloys, Int. J. Fatigue 146 (2021) 106165, https://doi.org/10.1016/J.IJFATIGUE.2021.106165.

[103] Z. Wu, S. Wu, J. Bao, W. Qian, S. Karabal, W. Sun, P.J. Withers, The effect of defect population on the anisotropic fatigue resistance of AlSi10Mg alloy fabricated by laser powder bed fusion, Int. J. Fatigue 151 (2021) 106317, https://doi.org/10.1016/J.IJFATIGUE.2021.106317.

[104] F. Sausto, P.E. Carrion, N. Shamsaei, S. Beretta, Fatigue failure mechanisms for AlSi10Mg manufactured by L-PBF under axial and torsional loads: the role of defects and residual stresses, Int. J. Fatigue 162 (2022) 106903, https://doi.org/10.1016/J.IJFATIGUE.2022.106903.

[105] Y. Zhang, X. Li, S. Yuan, R. Sun, T. Sakai, M.I. Lashari, U. Hamid, W. Li, High-cycle-fatigue properties of selective-laser-melted AlSi10Mg with multiple building directions, Int. J. Mech. Sci. 224 (2022) 107336, https://doi.org/10.1016/J.IJMECSCI.2022.107336.

[106] N.T. Aboulkhair, I. Maskery, C. Tuck, I. Ashcroft, N.M. Everitt, Improving the fatigue behaviour of a selectively laser melted aluminium alloy: Influence of heat treatment and surface quality, Mater. Des. 104 (2016) 174–182, https://doi.org/10.1016/J.MATDES.2016.05.041.

[107] Z.W. Xu, Q. Wang, X.S. Wang, C.H. Tan, M.H. Guo, P.B. Gao, High cycle fatigue performance of AlSi10Mg alloy produced by selective laser melting, Mech. Mater. 148 (2020) 103499, https://doi.org/10.1016/J.MECHMAT.2020.103499.

[108] S. Beretta, L. Patriarca, M. Gargourimotlagh, A. Hardaker, D. Brackett, M. Salimian, J. Gumpinger, T. Ghidini, A benchmark activity on the fatigue life assessment of AlSi10Mg components manufactured by L-PBF, Mater. Des. 218 (2022) 110713, https://doi.org/10.1016/J.MATDES.2022.110713.

[109] J.G. Santos Macías, C. Elangeswaran, L. Zhao, J.Y. Buffière, B. Van Hooreweder, A. Simar, Fatigue crack nucleation and growth in laser powder bed fusion AlSi10Mg under as built and post-treated conditions, Mater. Des. (2021) 110084, https://doi.org/10.1016/J.MATDES.2021.110084.

[110] M.S. Bisht, V. Gaur, I.V. Singh, On mechanical properties of SLM Al–Si alloy: Role of heat treatment-induced evolution of silicon morphology, Mater. Sci. Eng. A 858 (2022) 144157, https://doi.org/10.1016/J.MSEA.2022.144157.

[111] N.O. Larrosa, W. Wang, N. Read, M.H. Loretto, C. Evans, J. Carr, U. Tradowsky, M.M. Attallah, P.J. Withers, Linking microstructure and processing defects to mechanical properties of selectively laser melted AlSi10Mg alloy, Theor. Appl. Fract. Mech. 98 (2018) 123–133, https://doi.org/10.1016/J.TAFMEC.2018.09.011.

[112] J.N. Domfang Ngnekou, Y. Nadot, G. Henaff, J. Nicolai, L. Ridosz, Effect of as-built and ground surfaces on the fatigue properties of AlSi10Mg alloy produced by additive manufacturing, Metals (basel) 11 (2021), https://doi.org/10.3390/met11091432.

[113] F. Sausto, C. Tezzele, S. Beretta, Analysis of Fatigue Strength of L-PBF AlSi10Mg with Different Surface Post-Processes: effect of Residual Stresses, Metals (basel). 12 (2022), https://doi.org/10.3390/met12060898.

[114] W. Qian, S. Wu, Z. Wu, S. Ahmed, W. Zhang, G. Qian, P.J. Withers, In situ X-ray imaging of fatigue crack growth from multiple defects in additively manufactured AlSi10Mg alloy, Int. J. Fatigue 155 (2022) 106616, https://doi.org/10.1016/J.IJFATIGUE.2021.106616.

[115] R. Shrestha, J. Simsiriwong, N. Shamsaei, Fatigue behavior of additive manufactured 316L stainless steel parts: Effects of layer orientation and surface roughness, Addit. Manuf. 28 (2019), https://doi.org/10.1016/j.addma.2019.04.011.

[116] F. Stern, L. Becker, C. Cui, J. Tenkamp, V. Uhlenwinkel, M. Steinbacher, J. Boes, J. Lentz, R. Fechte-Heinen, S. Weber, F. Walther, Improving the defect Tolerance of PBF-LB/M Processed 316L Steel by increasing the Nitrogen Content, Adv. Eng. Mater. 25 (2023), https://doi.org/10.1002/adem.202200751.

[117] W.J. Lai, A. Ojha, Z. Li, C. Engler-Pinto, X. Su, Effect of residual stress on fatigue strength of 316L stainless steel produced by laser powder bed fusion process, Prog. Addit. Manuf. 6 (2021), https://doi.org/10.1007/s40964-021-00164-8.
[118] P. Kumar, R. Jayaraj, J. Suryawanshi, U.R. Satwik, J. McKinnell, U. Ramamurty, Fatigue strength of additively manufactured 316L austenitic stainless steel, Acta Mater. 199 (2020), https://doi.org/10.1016/j.actamat.2020.08.033.
[119] G.S. Ponticelli, R. Panciroli, S. Venettacci, F. Tagliaferri, S. Guarino, Experimental investigation on the fatigue behavior of laser powder bed fused 316L stainless steel, CIRP J. Manuf. Sci. Technol. 38 (2022), https://doi.org/10.1016/j.cirpj.2022.07.007.
[120] R. Shrestha, J. Simsiriwong, N. Shamsaei, Fatigue behavior of additive manufactured 316L stainless steel under axial versus rotating-bending loading: Synergistic effects of stress gradient, surface roughness, and volumetric defects, Int. J. Fatigue 144 (2021), https://doi.org/10.1016/j.ijfatigue.2020.106063.
[121] D. Kotzem, S. Kleszczynski, F. Stern, A. Elspaß, J. Tenkamp, G. Witt, F. Walther, Impact of single structural voids on fatigue properties of AISI 316L manufactured by laser powder bed fusion, Int. J. Fatigue 148 (2021), https://doi.org/10.1016/j.ijfatigue.2021.106207.
[122] X. Liang, A. Hor, C. Robert, M. Salem, F. Lin, F. Morel, High cycle fatigue behavior of 316L steel fabricated by laser powder bed fusion: Effects of surface defect and loading mode, Int. J. Fatigue 160 (2022), https://doi.org/10.1016/j.ijfatigue.2022.106843.
[123] F. Zeng, Y. Yang, G. Qian, Fatigue properties and S-N curve estimating of 316L stainless steel prepared by SLM, Int. J. Fatigue 162 (2022), https://doi.org/10.1016/j.ijfatigue.2022.106946.
[124] J. Nafar Dastgerdi, O. Jaberi, H. Remes, Influence of internal and surface defects on the fatigue performance of additively manufactured stainless steel 316L, Int. J. Fatigue 163 (2022), https://doi.org/10.1016/j.ijfatigue.2022.107025.
[125] C. Yu, P. Zhang, Z. Zhang, W. Liu, Microstructure and fatigue behavior of laser-powder bed fusion austenitic stainless steel, J. Mater. Sci. Technol. 46 (2020), https://doi.org/10.1016/j.jmst.2019.08.047.
[126] L. Cui, D. Deng, F. Jiang, R.L. Peng, T. Xin, R.T. Mousavian, Z. Yang, J. Moverare, Superior low cycle fatigue property from cell structures in additively manufactured 316L stainless steel, J. Mater. Sci. Technol. 111 (2022), https://doi.org/10.1016/j.jmst.2021.10.006.
[127] K. Malekipour, M. Mashayekhi, M. Badrossamay, Meso-scale damage mechanics modeling for high cycle fatigue behavior of additively manufactured components, Mech. Mater. 160 (2021), https://doi.org/10.1016/j.mechmat.2021.103951.
[128] E. Uhlmann, C. Fleck, G. Gerlitzky, F. Faltin, Dynamical Fatigue Behavior of Additive Manufactured Products for a Fundamental Life cycle Approach, Procedia CIRP (2017), https://doi.org/10.1016/j.procir.2016.11.138.
[129] B. Voloskov, S. Evlashin, S. Dagesyan, S. Abaimov, I. Akhatov, I. Sergeichev, Very high cycle fatigue behavior of additively manufactured 316L stainless steel, Materials 13 (2020), https://doi.org/10.3390/ma13153293.